





Probing the topological character of superconductors via nonlocal Hanbury Brown and Twiss correlations

Tusaradri Mohapatra , Subhajit Pal , and Colin Benjamin *

School of Physical Sciences, National Institute of Science Education & Research, HBNI, Jatni-752050, India and Homi Bhabha National Institute, Training School Complex, Anushaktinagar, Mumbai 400094, India

 (Received 29 March 2021; revised 2 August 2022; accepted 15 August 2022; published 6 September 2022)

Superconductors can be classified as topological or not based on whether time-reversal symmetry, chiral symmetry, and particle-hole symmetry are preserved or not. Further, topological superconductors can also be classified as chiral or helical. In this paper, using Hanbury Brown and Twiss (HBT) shot-noise correlations and the nonlocal conductance, we probe metal and two-dimensional unconventional superconductor and metal junctions to understand better the pairing topological vs nontopological or helical vs chiral or nodal vs gapful. We see that HBT correlations are asymmetric as a function of bias voltage for nontopological superconductors, whereas they are symmetric for topological superconductors irrespective of the barrier strength. Topological superconductors are associated with Majorana fermions which are important for topological quantum computation. By distinguishing topological superconductors from nontopological superconductors, our study will help search for Majorana fermions, which will aid in designing a topological quantum computer.

DOI: [10.1103/PhysRevB.106.125402](https://doi.org/10.1103/PhysRevB.106.125402)

I. INTRODUCTION

Conventional spin-singlet s -wave superconductors have spherically symmetric order parameters wherein pairing potential is independent of the direction of incident electrons. Any deviation from this is defined as an unconventional superconductor, e.g., p wave or d wave [1]. In two-dimensional (2D) unconventional superconductors, zero-bias conductance peak (ZBCP) may indicate the presence of Majorana zero modes and thus indicate the topological character of superconductors [2,3], but does not provide sufficient evidence for the pairing symmetry of the topological superconductor. ZBCP can not distinguish pairing symmetries of different topological superconductors, e.g., chiral d , chiral p , or helical p . Moreover, distinguishing different topological pairings is important as topological superconductors are building blocks of Majorana zero modes, potentially crucial in topological quantum computation [4,5].

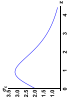
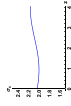
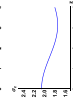
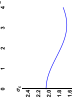
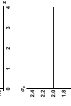
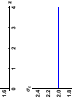
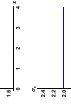
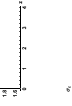
Among the many proposals to detect pairing symmetry of unconventional superconductors, a well-known method is the Knight shift measurement in a nuclear magnetic resonance (NMR) experiment [6]. Invariance of the Knight shift to change in temperature below T_c is strongly suggestive of spin-triplet pairing [7], e.g., chiral p , and distinguishes it from the spin-singlet pairing, e.g., chiral d . Now, both chiral p and chiral d are topological superconductors. Nevertheless, how do we distinguish chiral p from chiral d or helical p ? A different method, the current and magnetic field inversion (CFI) symmetry test of time-reversal symmetry (TRS), can be used to discriminate between chiral and helical superconductors, as CFI preserves TRS for helical superconductors.

At the same time, it breaks TRS for chiral superconductors [8]. However, these tests are not 100% full proof, so we propose two additional tests, the nonlocal differential shot-noise cross correlations and nonlocal Hanbury Brown and Twiss (HBT) correlations in metal and 2D unconventional superconductor and metal junctions, to distinguish between topological (chiral p , chiral d , helical p , $p_x\hat{x}$, and $p_x\hat{y}$) and nontopological (s , $p_x\hat{z}$, $d_{x^2-y^2}$, and d_{xy}) based on whether spin-rotational symmetry is present or not in 2D. Among these, chiral p , chiral d , helical p , and s wave are gapful, while $p_x\hat{x}$, $p_x\hat{y}$, $p_x\hat{z}$, d_{xy} , and $d_{x^2-y^2}$ are nodal. As shown in Ref. [9], different pairing symmetries of superconductors have been categorized as topological or nontopological via tenfold classification. As far as we are aware, shot-noise correlations have not yet been used to identify pairing symmetries of nodal triplet superconductors, such as $p_x\hat{x}$, $p_x\hat{y}$, or $p_x\hat{z}$. Hence, we also include these pairing symmetries in our study with HBT noise to distinguish topological from nontopological pairings and gapful from nodal. To decipher the pairing symmetry of unconventional superconductors, quantum transport in superconducting hybrid junctions via measurement of nonlocal differential conductance has been helpful [10]. However, shot-noise or nonlocal HBT correlations can give more information about the Cooper-pair splitting, which may help differentiate between pairing symmetries of 2D unconventional superconductors. We not only focus on cross correlations but also extend our study to differential shot-noise cross correlations.

The key take-home messages of our study are that HBT or shot-noise correlations are asymmetric as a function of bias voltage for nontopological superconductors. In contrast, they are symmetric for topological superconductors irrespective of the barrier strength. Further, we show how different topological pairings like nodal or gapful and chiral or helical can be distinguished from each other via the sign of HBT correlations

*colin.nano@gmail.com

TABLE I. Pairing symmetries of 2D unconventional superconductors with examples. The examples are from experimental papers where such pairing is the most likely. It is by no means complete confirmation. Herein lies the motivation of our work, which is to provide another method to probe the pairing symmetry of unconventional superconductors unambiguously.

Topology of 2D superconductors	Type	Pairing	Parity	Symmetry classification [9]	$\mathbf{d}(\mathbf{k})$	$\mathbf{d}(\theta)$	$\psi(\mathbf{k})$	$\psi(\theta)$	σ_c vs z	Examples
Nontopological	Gapful	s	Even	CI	0	0	1	1		Al, Pb [11]
	Nodal	$p_x \hat{z}$	Odd	AIII	$k_x \hat{z}$	$\cos \theta \hat{z}$	0	0		
		$d_{x^2-y^2}$	Even	CI	0	0	$k_x^2 - k_y^2$	$\cos 2\theta$		YBa ₂ Cu ₃ O _{7-δ} [12]
Topological	Chiral	d_{xy}	Even	CI	0	0	$2k_x k_y$	$2 \cos \theta \sin \theta$		FeSe _{1-x} S _x [13]
		$p_x + ip_y$	Odd	D	$(k_x + ik_y) \hat{z}$	$e^{i\theta} \hat{z}$	0	0		Possibly Sr ₂ RuO ₄ [6], UTe ₂ [14]
	(Gapful)	$d_{x^2-y^2} + id_{xy}$	Even	C	0	0	$k_x^2 - k_y^2 + i2k_x k_y$	$e^{i2\theta}$		SrPtAs [15]
	Helical (Gapful)	p	odd [16]	DIII	$\hat{x}k_y - \hat{y}k_x$	$\sin \theta \hat{x} - \cos \theta \hat{y}$	0	0		Possibly Sr ₂ RuO ₄ [6]
	Nodal	$p_x \hat{x}, p_x \hat{y}$	odd [16]	DIII	$k_x \hat{x}, k_x \hat{y}$	$\cos \theta \hat{x}, \cos \theta \hat{y}$	0	0		

or their zero-bias nature for both transparent and tunneling interfaces. Both differential shot-noise and HBT correlations thus serve as effective tools to discriminate between pairing symmetries which we explain in detail in this paper.

The paper is organized as follows: We give an overview of the possible pairing symmetries of 2D unconventional superconductors in Sec. II. Section III deals with the 2D BTK approach and how it is used to calculate differential shot-noise correlations, shot-noise cross correlations, and nonlocal conductance in our setup. Next, in Sec. IV we describe our setup, which is a 2D normal metal/insulator/unconventional superconductor/insulator/normal metal ($N_1/I/US/I/N_2$) junction for each pairing symmetry. We then discuss the respective wave functions and boundary conditions necessary to calculate nonlocal conductance, and shot noise, i.e., HBT correlations and differential shot-noise correlations. It is followed by a discussion on the results, first for nonlocal conductance and differential shot-noise cross correlations and then for HBT cross correlations. Finally, we provide a discussion on why we see what we see and summarize how different processes contribute to HBT correlations in the subsection ‘‘Processes in Play’’ via Tables II and III. We finally conclude with a comparison between different pairing symmetries: topological (gapful helical vs gapful chiral vs nodal) vs nontopological using HBT as well as differential shot-noise cross correlations in Tables IV and V. In the Appendix, we have elaborated first on the crossed Andreev conductance and elastic cotunneling and then in detail on the components of shot-noise cross correlations.

II. PAIRING SYMMETRIES

The pairing symmetry of superconductors is classified based on spin angular momentum (S) of Cooper pairs, which form via pairing between two spin-half electrons. It can be either singlet (0) or triplet (1). Spin-singlet states are antisymmetric in spin space, while spin-triplet states are symmetric. Column 4 in Table I describes the parity of the different symmetries. In the absence of spin-orbit coupling, pairing symmetries are either even parity (spin singlet) or odd parity (spin triplet). Pairing symmetries, as mentioned in Table I, that satisfy $\psi(\mathbf{k}) = \psi(-\mathbf{k})$ are associated with spin-singlet (even-parity) superconductors, and $\mathbf{d}(\mathbf{k}) = -\mathbf{d}(-\mathbf{k})$ are associated with spin-triplet (odd-parity) superconductors [16]. The presence of the spin-orbit coupling term breaks the inversion symmetry. For superconductors with pairing, gapful (helical- p) and nodal ($p_x\hat{x}$, $p_x\hat{y}$), there is a spin-orbit coupling term, which too breaks the inversion symmetry. When the orbital part of the wave function is even, it is denoted as even parity with orbital angular momentum ($L = 0, 2, 4 \dots$). When the orbital part is odd, it is called odd parity with orbital angular momentum ($L = 1, 3, 5 \dots$). The total wave function of the Cooper pair must be antisymmetric under the exchange of particles. Thus, either the orbital part is antisymmetric and the spin part is symmetric or vice versa. Spin-singlet pairing is associated with even orbital angular momentum, and spin-triplet pairing is associated with odd orbital angular momentum [17]. Even-parity, spin-singlet Cooper-pair states with angular momentum $L = 0, 2$ are denoted as s wave and d wave while odd-parity, spin-triplet Cooper-pair states with

angular momentum $L = 1, 3$ are denoted as p wave and f wave.

Column 5 in Table I describes tenfold symmetry classification. Unconventional superconductors, in general, can be categorized as topological or nontopological based on the well-known tenfold symmetry classification. For 2D superconductors based on Bogoliubov–de Gennes Hamiltonian, pairing symmetries can be categorized into different symmetry classes [9] based on (1) spin-rotation symmetry, i.e., rotation about z component of spin, by the presence or absence of (2) time-reversal symmetry (TRS), (3) chiral symmetry also known as sublattice symmetry (SLS), and (4) particle-hole symmetry (PHS). For a system where TRS is present, $\hat{T} = \pm 1$ where \hat{T} is the TRS operator, and when TRS is absent, $\hat{T} = 0$. Similarly, when PHS is present, $\hat{P} = \pm 1$, \hat{P} being the PHS operator, and when PHS is absent, $\hat{P} = 0$. Chiral symmetry can be defined based on whether TRS and PHS are present or not. TRS and PHS together determine chirality or SLS. When SLS is present, $\hat{C} = 1$ (where \hat{C} is the chiral symmetry operator), and when absent, $\hat{C} = 0$. When either TRS or PHS is absent, SLS is absent $\hat{C} = 0$, which includes AI, AII, C, and D symmetry classes. When both TRS and PHS are present, SLS is present $\hat{C} = 1$, which includes CI, CII, BDI, and DIII symmetry classes. For a superconductor, if TRS and PHS are absent, but SLS holds, i.e., $\hat{C} = 1$, then it is classified as AIII symmetry, but if SLS is absent, i.e., $\hat{C} = 0$, then it is A symmetry class.

We first discuss nodal triplet pairing symmetries, e.g., $p_x\hat{x}$, $p_x\hat{y}$, and $p_x\hat{z}$. Among these, $p_x\hat{x}$ and $p_x\hat{y}$ do not possess spin-rotation symmetry but TRS, PHS, and SLS are present and therefore $p_x\hat{x}$ and $p_x\hat{y}$ belong to DIII symmetry class which is topological in 2D. However, when spin-rotation symmetry is present in case of a 2D superconductor, there is an exception for AIII symmetry class. AIII symmetry class is then uniquely defined by TRS and spin-rotation symmetry in 2D. Those materials for whom both spin-rotation symmetry S_z [spin-rotation symmetry SU(2) around z direction] and TRS are preserved, can also be classified as AIII symmetry class. In 2D superconductors, $p_x\hat{z}$ pairing is an example of an AIII symmetry class that possesses spin-rotation symmetry and preserves TRS. This is nontopological in 2D; see Refs. [9,18] for a detailed explanation. Nodal singlet pairing, such as d_{xy} and $d_{x^2-y^2}$, preserve TRS and possess spin-rotation symmetry. These are examples of 2D BDG Hamiltonian in CI symmetry class that preserves PHS and SLS and thus are nontopological in 2D.

Gapful pairing symmetries such as gapful triplet chiral- p pairing with \mathbf{d} parallel to z direction possess spin-rotation symmetry around fixed z axis and preserve PHS but TRS and SLS are absent and thus belong to the D symmetry class in 2D which is topological. Next, gapful singlet chiral- d pairing possesses complete spin-rotation symmetry. It preserves PHS, but TRS and SLS are absent and are an example of the C symmetry class in 2D, which is topological. Gapful triplet helical- p pairing preserves TRS and PHS but does not possess spin-rotation symmetry, but preserves SLS, and is a member of the DIII symmetry class in 2D, which is categorized as a gapful topological superconductor. Conventional s -wave superconductors are of the CI symmetry class. These possess complete spin-rotation symmetry and preserve both TRS and

PHS, thus preserving SLS, which is nontopological in 2D. For pairing cases without spin-rotation symmetry, there is small but finite Rashba spin-orbit coupling, and for cases with spin-rotation symmetry, there is zero Rashba spin-orbit coupling.

In columns 6–9 of Table I, pairing potential $[\hat{\Delta}(\mathbf{k})]$ of a Cooper pair is written in terms of $\mathbf{d}(\mathbf{k})$ for spin-triplet and a scalar term $\psi(\mathbf{k})$ for spin-singlet pairing. For spin-triplet pairing such as topological gapful (chiral p , chiral d , helical p) and nodal p_x pairing [10,19,20], pair potential is given as

$$\hat{\Delta}(\mathbf{k}) = \Delta(\mathbf{d}(\mathbf{k}) \cdot \hat{\sigma})i\sigma_2, \quad (1)$$

where $\mathbf{d}(\mathbf{k})$ is defined for each pairing symmetry in Table I, $\hat{\sigma} = \sigma_1\hat{x} + \sigma_2\hat{y} + \sigma_3\hat{z}$ where $\sigma_{1,2,3}$ are the three Pauli matrices, and Δ is the magnitude of the superconducting gap. For 2D superconductor, momentum components are $k_x = k_F \cos \theta$, $k_y = k_F \sin \theta$, where k_F is Fermi wave vector and θ is angle the incident electron makes with x axis.

$p_x\hat{z}$ pairing is a nodal nontopological superconductor with \mathbf{d} in \hat{z} direction, i.e., $\mathbf{d}(\mathbf{k}) = (k_x)\hat{z}/k_F = \cos \theta\hat{z}$. Spin-triplet p -wave states or chiral- p pairing has $\mathbf{d}(\mathbf{k}) = (k_x \pm ik_y)\hat{z}/k_F$ with $\mathbf{d} \parallel \hat{z}$, i.e., \mathbf{d} is parallel to crystal c axis [21], implying, $\mathbf{d}(\mathbf{k}) = (\cos \theta \pm i \sin \theta)\hat{z}$. In helical- p -wave superconductor, \mathbf{d} is defined as $(\hat{x}k_x \pm \hat{y}k_y)/k_F$ or $(\hat{x}k_y \pm \hat{y}k_x)/k_F$ with $\mathbf{d} \perp \hat{z}$ (\mathbf{d} in ab plane), i.e., \mathbf{d} is perpendicular to the crystal c axis [22], implying, $\mathbf{d}(\mathbf{k}) = (\hat{x} \cos \theta \pm \hat{y} \sin \theta)$ or $(\hat{x} \sin \theta \pm \hat{y} \cos \theta)$. For nodal topological p_x pairing, \mathbf{d} can be in \hat{x} or \hat{y} direction, i.e., $\mathbf{d}(\mathbf{k}) = k_x\hat{x}/k_F = \cos(\theta)\hat{x}$ or $\mathbf{d}(\mathbf{k}) = k_y\hat{y}/k_F = \cos(\theta)\hat{y}$.

For spin-singlet pairing such as nontopological gapful s , nontopological nodal $d_{x^2-y^2}$ and d_{xy} , topological gapful chiral- d pairing [20,23], the pair potential is given as

$$\Delta(\mathbf{k}) = \Delta(\psi(\mathbf{k})), \quad (2)$$

where $\psi(\mathbf{k})$ is a scalar term that represents spin-singlet pairing and is defined in Table I. s -wave superconductors are nontopological gapful superconductors [24]. $d_{x^2-y^2}$ pairing is a nodal nontopological superconductor, where the order parameter vanishes, diagonal to x, y directions [25] with $\psi(\mathbf{k}) = (k_x^2 - k_y^2)/k_F^2 = \cos 2\theta$. d_{xy} pairing is a nodal nontopological superconductor, where the order parameter vanishes in x, y direction [26] with $\psi(\mathbf{k}) = (2k_x k_y)/k_F^2 = 2 \cos \theta \sin \theta$. For chiral- d -wave superconductor, $\psi(\mathbf{k}) = [(k_x^2 - k_y^2) + i2k_x k_y]/k_F^2 = e^{i2\theta}$.

In Table I, column 10, we have plotted normalized conductance (σ_c) vs barrier strength (z) at zero bias for a metal and 2D superconductor junction which is a typical signature of the existence of Majorana bound states at metal and topological superconductor interface. Normalized conductance σ_c is quantized for topological superconductors, e.g., chiral- p , chiral- d , helical- p , $p_x\hat{x}$, and $p_x\hat{y}$ cases and is in line with the tenfold symmetry classification for 2D BDG Hamiltonian [9].

In Table I, column 11, examples of topological and nontopological superconductors are given with their respective pairing symmetries. Topological gapful superconductors are chiral p wave which are $p_x + ip_y$ superconductor [27] and chiral d wave which is $d_{x^2-y^2} + id_{xy}$ spin-singlet superconductor [28]. In Table I, we give examples of unconventional superconductors for which the said pairing is most likely. For example, the pairing symmetry of Sr_2RuO_4 is still inconclusive, as regards chiral p or helical p [6]. The next section explains the 2D BTK (Blonder, Tinkham, and Klapp-

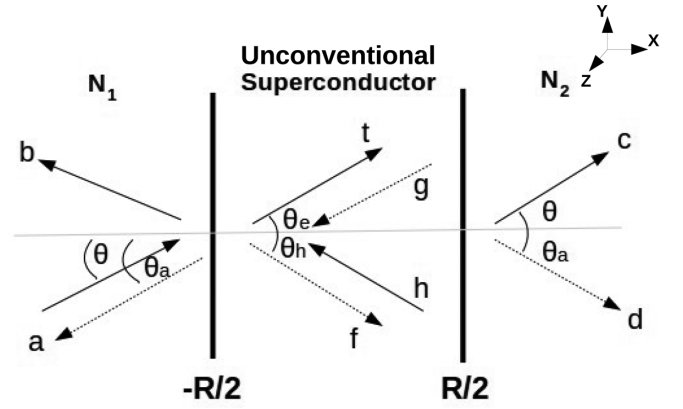


FIG. 1. Schematic illustration of reflection and transmission of electrons and holes in a $N_1/I/US/I/N_2$ junction in x - y plane. The solid line represents the scattering of electrons, while the dotted line represents the scattering of holes.

wijk) approach, and using it, we calculate HBT correlations and nonlocal conductance for the chosen 2D $N_1/I/US/I/N_2$ setup.

III. 2D BTK APPROACH

We consider a 2D $N_1/I/US/I/N_2$ junction (see Fig. 1) with insulators at $x = -R/2$ and $R/2$. θ is angle, the incident (transmitted) electrons (holes) make with x axis [29] in N_1 (N_2) region. θ_a is angle, reflected (transmitted) holes (electrons) make with x axis in N_1 (N_2) region. Finally, $\theta_{e(h)}$ is angle, transmitted electrons (holes) make with x axis in US region. We use the Andreev approximation in normal metal regions, which implies that the electron and hole wave vectors are identical and equal to the Fermi wave vector (k_F). We consider Andreev approximation in the US region for cases with spin-rotational symmetry (in the absence of Rashba spin-orbit coupling), which implies that electronlike quasiparticle and holelike quasiparticle wave vectors are equal to Fermi wave vector (k_F). In contrast, there is no Andreev approximation in the US region for cases without spin-rotational symmetry; here, Rashba spin-orbit coupling is finite. Due to presence of translational invariance in y direction [30], electron, hole, and quasiparticle wave vectors in y direction in N_1 , N_2 , and US regions are conserved. This further implies that $\theta = \theta_a = \theta_{e(h)}$.

In Fig. 1 Andreev reflection amplitude is denoted as $a = s_{11}^{eh}$, normal reflection amplitude as $b = s_{11}^{ee}$, transmission amplitude of elastic cotunneling $c = s_{12}^{ee}$, transmission amplitude of cross Andreev reflection $d = s_{12}^{eh}$. Scattering amplitude $s_{ik}^{\alpha\gamma}$ represents a particle α ($\in e, h$) incident from contact i ($\in N_1, N_2$) which is reflected or transmitted to contact k ($\in N_1, N_2$) as a particle γ ($\in e, h$). In Fig. 2 we show our chosen setting to study transport and current cross correlations across unconventional superconductors for a 2D $N_1/I/US/I/N_2$ junction wherein N_1 is at bias voltage V_1 and N_2 is at bias voltage V_2 while US is grounded.

A. Nonlocal conductance and shot noise

Andreev reflection can be nonlocal, too, known as crossed Andreev reflection (CAR), in which an electron is transmitted

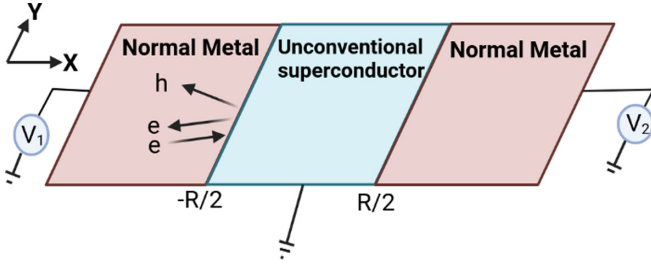


FIG. 2. 2D $N_1/I/US/I/N_2$ junction. The superconductor is grounded while bias voltage V_1 is applied to N_1 and V_2 is applied to N_2 . At $-R/2, R/2$ these are insulators which are represented by δ -function potentials.

as a hole through the other interface with a superconductor, i.e., spatially separated entangled electrons in both the normal metals [31]. When an electron (hole) from the left normal metal tunnels to the right normal metal as an electron (hole), the process is known as elastic cotunneling (EC).

First, we calculate nonlocal differential conductance, defined as conductance in N_2 when both N_2 and US are grounded, and voltage is applied to N_1 . The difference between CAR and elastic cotunneling (EC) in absence of any voltage bias to N_2 is defined as nonlocal differential conductance [31] $G_{NL} = G_{CAR} - G_{EC}$, where

$$G_{CAR} = \int_{-\pi/2}^{\pi/2} d\theta \frac{\cos \theta}{2\pi} |d|^2, \quad G_{EC} = \int_{-\pi/2}^{\pi/2} d\theta \frac{\cos \theta}{2\pi} |c|^2, \quad (3)$$

$d = s_{12}^{eh}$ is scattering amplitude for CAR while $c = s_{12}^{ee}$ is scattering amplitude for EC. Shot noise can give more information regarding the pairing symmetry from current cross correlations in the $N_1/I/US/I/N_2$ junction, which conductance cannot. It is why we look at cross correlations and differential shot-noise cross correlations. Discreteness of charge leads to nonequilibrium temporal fluctuations in the current known as shot noise. Even at zero temperature, shot noise exists, unlike thermal noise that originates due to finite temperature and vanishes at zero temperature [32].

The general result for shot-noise cross correlations using 2D BTK for our setup (see Fig. 2) includes an integral over incident angle θ and is given [33,34] as

$$S^{12} = \frac{2e^2}{h} \int_{-\pi/2}^{\pi/2} d\theta \frac{\cos \theta}{2\pi} \sum_{\substack{k,l \in 1,2, \\ x,y,\gamma,\delta \in e,h}} \text{sgn}(x)\text{sgn}(y) \\ \times \int W_{k,\gamma;l,\delta}(1x, E) \\ \times W_{l,\delta;k,\gamma}(2y, E) f_{k\gamma}(E) [1 - f_{l\delta}(E)] dE, \quad (4)$$

where parameter $W_{k,\gamma;l,\delta}(1x, E) = \delta_{1k} \delta_{1l} \delta_{x\gamma} \delta_{x\delta} - s_{1k}^{x\gamma*}(E) s_{1l}^{x\delta}(E)$ contains information about the scattering process. $s_{1k}^{x\gamma}(E)$ represents scattering amplitude, with γ denoting an electron or hole incident from contact k which is transmitted to N_1 as particle of type x . $f_{k\gamma}$ is Fermi function for particle of type γ in contact k . Normal metal N_1 is contact 1 while normal metal N_2 is contact 2. Here $\text{sgn}(x) = +1$ for $x = e$, i.e., electron, and $\text{sgn}(x) = -1$ for $x = h$, i.e., hole. In a previous study [35] it was shown that the sign of

cross correlations and sign of differential shot-noise cross correlations could be different for some regime of bias voltages applied. Taking a cue from this, we study both shot-noise cross correlations and differential shot-noise cross correlations. It will help us understand different pairing symmetries in our setup. The differential shot-noise cross correlations $\frac{dS^{12}}{dV}$ in symmetric setup ($V_1 = V_2 = V$) at zero temperature are given as [33,35]

$$\frac{dS^{12}(V_1 = V_2 = V)}{dV} = \frac{4|e|^3}{h} \text{sgn}(|e|V) \int_{-\pi/2}^{\pi/2} d\theta \frac{\cos \theta}{2\pi} (-s_A + s_B), \quad (5)$$

where $s_A = \sum_{\alpha=a,b,c,d} [s_\alpha(|e|V) + s_\alpha(-|e|V)]$, with

$$s_a = s_{21}^{eh} s_{12}^{he} s_{11}^{hh*} s_{22}^{ee*} + s_{12}^{eh} s_{21}^{he} s_{11}^{hh*} s_{22}^{ee*}, \\ s_b = s_{12}^{hh} s_{21}^{ee} s_{22}^{ee*} s_{11}^{hh*} + s_{12}^{ee} s_{21}^{hh} s_{11}^{hh*} s_{22}^{ee*}, \\ s_c = s_{11}^{hh} s_{21}^{ee} s_{21}^{ee*} s_{11}^{hh*} + s_{11}^{ee} s_{21}^{hh} s_{21}^{hh*} s_{11}^{ee*}, \\ s_d = s_{12}^{eh} s_{22}^{ee*} s_{12}^{hh*} + s_{12}^{hh} s_{22}^{ee} s_{12}^{ee*} s_{22}^{hh*},$$

and $s_B = \sum_{\alpha=e,f,g,h} [s_\alpha(|e|V) + s_\alpha(-|e|V)]$, with

$$s_e = s_{12}^{ee} s_{21}^{eh} s_{22}^{ee*} s_{11}^{hh*} + s_{21}^{hh} s_{12}^{he} s_{11}^{hh*} s_{22}^{ee*}, \\ s_f = s_{12}^{eh} s_{21}^{ee} s_{11}^{hh*} s_{22}^{ee*} + s_{12}^{hh} s_{21}^{he} s_{11}^{hh*} s_{22}^{ee*}, \\ s_g = s_{11}^{eh} s_{21}^{ee} s_{11}^{hh*} s_{21}^{ee*} + s_{21}^{hh} s_{11}^{he} s_{11}^{hh*} s_{21}^{ee*}, \\ s_h = s_{12}^{ee} s_{12}^{eh} s_{22}^{ee*} s_{12}^{hh*} + s_{12}^{eh} s_{12}^{he} s_{22}^{ee*} s_{12}^{hh*}.$$

The differential shot-noise cross correlations in nonlocal setup at zero temperature with bias voltage $V_1 = V$ applied to N_1 while N_2 grounded is given by

$$\frac{dS^{12}(V_1 = V, V_2 = 0)}{dV} = \frac{4|e|^3}{h} \text{sgn}(|e|V) \int_{-\pi/2}^{\pi/2} d\theta \frac{\cos \theta}{2\pi} (-s_C + s_D), \quad (6)$$

where $s_C = s_m(-|e|V) + s_n(|e|V) + s_c(|e|V) + s_c(-|e|V) + s_i(|e|V) + s_j(-|e|V)$, and $s_D = s_e(|e|V) + s_g(|e|V) + s_g(-|e|V) + s_k(|e|V) + s_l(-|e|V) + s_f(-|e|V)$ with

$$s_m = s_{21}^{eh} s_{12}^{he} s_{11}^{hh*} s_{22}^{ee*} + s_{12}^{ee} s_{21}^{hh} s_{11}^{hh*} s_{22}^{ee*}, \\ s_n = s_{12}^{eh} s_{21}^{ee} s_{11}^{hh*} s_{22}^{ee*} + s_{12}^{hh} s_{21}^{he} s_{11}^{hh*} s_{22}^{ee*}, \\ s_i = s_{12}^{ee} s_{21}^{he} s_{11}^{hh*} s_{22}^{ee*} + s_{21}^{hh} s_{12}^{ee} s_{11}^{hh*} s_{22}^{ee*}, \\ s_j = s_{12}^{eh} s_{21}^{hh} s_{11}^{hh*} s_{22}^{ee*} + s_{12}^{hh} s_{21}^{eh} s_{11}^{hh*} s_{22}^{ee*}, \\ s_k = s_{12}^{ee} s_{21}^{ee} s_{11}^{hh*} s_{22}^{ee*} + s_{21}^{hh} s_{12}^{he} s_{11}^{hh*} s_{22}^{ee*}, \\ s_l = s_{12}^{hh} s_{21}^{hh} s_{11}^{hh*} s_{22}^{ee*} + s_{12}^{eh} s_{21}^{he} s_{11}^{hh*} s_{22}^{ee*}.$$

The nonlocal conductance and shot-noise results for normal incidence ($\theta = 0$) agree with 1D BTK results [36]. In the next section, we write the wave functions and boundary conditions for the $N_1/I/US/I/N_2$ junctions, first for pairing symmetries that possess spin-rotation symmetries, followed by pairing symmetries that do not possess spin-rotation symmetry.

IV. THEORY

We first discuss the wave functions for pairing symmetries with spin-rotation symmetry, i.e., s wave, d_{xy} , $d_{x^2-y^2}$, $p_x\hat{z}$, chiral p , and chiral d followed by their boundary conditions. Next, we discuss wave functions for pairing symmetries that do not possess spin-rotation symmetry, i.e., $p_x\hat{x}$, $p_x\hat{y}$, and helical p followed by their boundary conditions.

A. With spin rotation symmetry

The 2D Hamiltonian for BDG equation $\mathcal{H}\psi = E\psi$ for US which possesses full spin-rotation symmetry, i.e., for pairing symmetries d_{xy} , $d_{x^2-y^2}$, s -wave, and chiral- d pairing and finally with fixed spin-rotation symmetry around z axis, i.e., $p_x\hat{z}$, chiral- p pairing, is a 2×2 matrix [9,10], and is written

$$\begin{aligned} \psi_{N_1}(x) &= e^{ik_F y \sin \theta} \left[\begin{pmatrix} 1 \\ 0 \end{pmatrix} (e^{ik_x x} + b e^{-ik_x x}) + a \begin{pmatrix} 0 \\ 1 \end{pmatrix} e^{ik_x x} \right] \quad \text{for } x < -\frac{R}{2}, \\ \psi_{US}(x) &= e^{ik_F y \sin \theta} \left[\begin{pmatrix} u(\theta) \\ \eta^*(\theta)v(\theta) \end{pmatrix} t e^{ik_x(x+\frac{R}{2})} e^{-(x+\frac{R}{2})/\xi} + \begin{pmatrix} \eta(\theta)v(\theta) \\ u(\theta) \end{pmatrix} f e^{-ik_x(x+\frac{R}{2})} e^{-(x+\frac{R}{2})/\xi} + \begin{pmatrix} u(\theta_-) \\ \eta^*(\theta_-)v(\theta_-) \end{pmatrix} \right. \\ &\quad \left. \times g e^{-ik_x(x-\frac{R}{2})} e^{(x-\frac{R}{2})/\xi} + \begin{pmatrix} \eta(\theta_-)v(\theta_-) \\ u(\theta_-) \end{pmatrix} h e^{ik_x(x-\frac{R}{2})} e^{(x-\frac{R}{2})/\xi} \right] \quad \text{for } -\frac{R}{2} < x < \frac{R}{2}, \\ \psi_{N_2}(x) &= e^{ik_F y \sin \theta} \left[c \begin{pmatrix} 1 \\ 0 \end{pmatrix} e^{ik_x(x-\frac{R}{2})} + d \begin{pmatrix} 0 \\ 1 \end{pmatrix} e^{-ik_x(x-\frac{R}{2})} \right] \quad \text{for } x > R/2, \end{aligned} \quad (8)$$

where $\eta(\theta_{\pm}) = \Delta(\theta_{\pm})/|\Delta(\theta_{\pm})|$ with $\theta_+ = \theta$ and $\theta_- = \pi - \theta$. $\Delta(\mathbf{k}, x) = \Delta$ from Eq. (2) is constant in s -wave superconducting region and is zero in the normal-metal regions. For gapful chiral- p superconductor [10], the pair potential is $\Delta(\theta_{\pm}) = \Delta e^{i\theta_{\pm}}$ and for gapful chiral- d superconductor, $\Delta(\theta_{\pm}) = \Delta e^{2i\theta_{\pm}}$. For nodal $d_{x^2-y^2}$ superconductor, pairing potential is $\Delta(\theta_{\pm}) = \Delta \cos(2\theta_{\pm}) = \Delta \cos(2\theta)$, for d_{xy} superconductor, $\Delta(\theta_{\pm}) = 2\Delta \cos(\theta_{\pm}) \sin(\theta_{\pm}) = \pm 2\Delta \cos(\theta) \sin(\theta)$, and for $p_x\hat{z}$ superconductor, $\Delta(\theta_{\pm}) = \Delta \cos(\theta_{\pm}) = \pm \Delta \cos(\theta)$. The coherence factors are $u(\theta_{\pm}) = \sqrt{[E + \sqrt{E^2 - |\Delta(\theta_{\pm})|^2}]/(2E)}$ and $v(\theta_{\pm}) = \sqrt{[E - \sqrt{E^2 - |\Delta(\theta_{\pm})|^2}]/(2E)}$.

1. Boundary conditions

For pairing symmetries that possess spin-rotation symmetry, i.e., \mathbf{d} is in z direction with finite d_z for spin-triplet superconductors, e.g., $p_x\hat{z}$, chiral p , and for full spin-rotation symmetry with scalar ψ for spin-singlet superconductors, e.g., s wave, d_{xy} , $d_{x^2-y^2}$, and chiral d , pairing potential is a scalar term. The continuity equation and current conservation at interface lead to boundary conditions as mentioned in Eq. (9), solving these one can calculate the scattering amplitudes [37]. The general boundary conditions at the interfaces for a $N_1/I/US/I/N_2$ junction, where US satisfies spin-rotation

as

$$\mathcal{H} = \begin{pmatrix} H_0(\mathbf{k}) & \Delta(\mathbf{k}) \\ \Delta^\dagger(\mathbf{k}) & -H_0^*(-\mathbf{k}) \end{pmatrix}, \quad (7)$$

with eigenspinor (c_k^\dagger, c_{-k}) , where c_k^\dagger (c_{-k}) being the creation (annihilation) operators. Pairing potential for triplet pairing is $\Delta(\mathbf{k}) = \Delta d_z(k)$ for $p_x\hat{z}$ and chiral- p cases as defined in Eq. (1), and in terms of $\psi(\mathbf{k})$ for singlet as $\Delta(\mathbf{k}) = \Delta\psi(k)$, i.e., d_{xy} , $d_{x^2-y^2}$, s -wave, chiral- d cases, is defined in Eq. (2). Pairing symmetries that satisfy $\Delta(\mathbf{k}) = \Delta(-\mathbf{k})$ are spin-singlet (even-parity) superconductors [16] for cases with spin-rotation symmetry in the absence of Rashba spin-orbit coupling. In Eq. (7), $H_0(\mathbf{k}) = (-\frac{\hbar^2 k^2}{2m} + U(x) - E_F)$, wave functions in N_1 , US, and N_2 regions for d_{xy} , $d_{x^2-y^2}$, s -wave, chiral- p , chiral- d , and $p_x\hat{z}$ pairing, and for an electron incident from N_1 are given as

symmetry at $x = -R/2$ and $R/2$ are given by

$$\begin{aligned} \Psi_{N_1}|_{x=-R/2} &= \Psi_{US}|_{x=-R/2}, \quad \Psi_{US}|_{x=R/2} = \Psi_{N_2}|_{x=R/2}, \\ \frac{\partial}{\partial x}(\Psi_{US} - \Psi_{N_1})|_{x=-R/2} &= (2mU_1/\hbar^2)\Psi_{N_1}|_{x=-R/2}, \\ \frac{\partial}{\partial x}(\Psi_{N_2} - \Psi_{US})|_{x=R/2} &= (2mU_2/\hbar^2)\Psi_{US}|_{x=R/2}. \end{aligned} \quad (9)$$

The barrier strength at the interface in both Eqs. (12) and (9) is characterized by dimensionless parameters $z_i = 2mU_i/\hbar^2 k_F$, $i = 1, 2$. From the scattering amplitudes $a = s_{11}^{eh}$, $b = s_{11}^{ee}$, $c = s_{12}^{ee}$, $d = s_{12}^{eh}$, we obtain Andreev and normal reflection probabilities as $A = |a|^2$ and $B = |b|^2$. $C = |c|^2$ and $D = |d|^2$ define probabilities for electron cotunneling (EC) and crossed Andreev reflection (CAR), respectively. This paper considers interface barrier strengths $z = z_1 = z_2$.

B. Without spin-rotation symmetry

We adopt the Bogoliubov-de Gennes (BDG) approach to study the transport in $N_1/I/US/I/N_2$ junction. The 2D Hamiltonian for BDG equation $\mathcal{H}\psi = E\psi$ without spin-rotation symmetry in case of $p_x\hat{x}$, $p_x\hat{y}$, and helical- p pairing [9] can be written as

$$\mathcal{H} = \begin{pmatrix} H(\mathbf{k}) & \hat{\Delta}(\mathbf{k}) \\ \hat{\Delta}^\dagger(\mathbf{k}) & -H^*(-\mathbf{k}) \end{pmatrix}, \quad (10)$$

with eigenspinor $(c_{k\uparrow}^\dagger, c_{k\downarrow}^\dagger, c_{-k\uparrow}, c_{-k\downarrow})$ of \mathcal{H} , where $c_{k\uparrow}^\dagger$ ($c_{-k\uparrow}$) denotes creation (annihilation) operator of spin-up quasiparticle and $c_{k\downarrow}^\dagger$ ($c_{-k\downarrow}$) denotes creation (annihilation) operator of spin-down quasiparticle. Pairing potential $\hat{\Delta}(k)$ for spin-triplet cases ($p_x\hat{x}$, $p_x\hat{y}$, and helical- p) is defined via Eq. (1) and $H(\mathbf{k}) = H_0(\mathbf{k}) \cdot \sigma_0 + H_p(\mathbf{k})$ with $H_0(\mathbf{k}) = (-\frac{\hbar^2 k^2}{2m} + U(x) - E_F)$, $H_p(\mathbf{k}) = \mathbf{V}(\mathbf{k}) \cdot \hat{\sigma}$ denotes the spin-orbit coupling term and $\mathbf{k} = (k_x, k_y, 0)$. Here σ_0 is 2×2 identity matrix and $\hat{\sigma} = \sigma_1\hat{x} + \sigma_2\hat{y} + \sigma_3\hat{z}$ where $\sigma_{1,2,3}$ are the three Pauli matrices. As in [22], $\mathbf{V}(\mathbf{k}) = \lambda(\hat{x}k_y - \hat{y}k_x)$ with Rashba spin-orbit coupling constant λ . In H_0 , $U(x) = U_1\delta(x + R/2) + U_2\delta(x - R/2)$ with U_1 and U_2 being the barrier strengths and R is the

thickness in x direction of 2D US lying in the x - y plane. The excitation energy E is measured relative to Fermi energy E_F , and m is the electronlike or holelike quasiparticle mass. For simplicity, we neglect self-consistency of the spatial distribution of the pair potential in the US. In the presence of Rashba spin-orbit coupling for $\lambda \neq 0$, the additional term $H_p(\mathbf{k})$ in Hamiltonian breaks the inversion symmetry, i.e., $H_p(\mathbf{k}) = -H_p(-\mathbf{k})$ and $\hat{\Delta}(\mathbf{k}) = -\hat{\Delta}(-\mathbf{k})$ for odd-parity superconductors, i.e., helical p , $p_x\hat{x}$, and $p_x\hat{y}$. However, mixed-parity states like noncentrosymmetry superconductors (NCS), e.g., helical- $p + s$, have no definite parity [38], i.e., $\hat{\Delta}(\mathbf{k}) \neq \pm\hat{\Delta}(-\mathbf{k})$.

The wave functions in N_1 , US, and N_2 regions for an electron incident from N_1 are

$$\begin{aligned} \psi_{N_1}(x) &= e^{ik_y y} \left[\begin{pmatrix} 1 \\ 0 \\ 0 \\ 0 \end{pmatrix} (e^{ik_x x} + b_1 e^{-ik_x x}) + b_2 \begin{pmatrix} 1 \\ 0 \\ 0 \\ 0 \end{pmatrix} e^{-ik_x x} + a_1 \begin{pmatrix} 0 \\ 0 \\ 1 \\ 0 \end{pmatrix} e^{ik_x x} + a_2 \begin{pmatrix} 0 \\ 0 \\ 0 \\ 1 \end{pmatrix} e^{ik_x x} \right] \quad \text{for } x < -\frac{R}{2}, \\ \psi_{US}(x) &= e^{ik_y y} \left\{ \begin{aligned} &t_1 \begin{pmatrix} u \\ -i\alpha_1^{-1}u \\ i\alpha_1^{-1}v \\ v \end{pmatrix} e^{ik_{\uparrow x}^e(x+\frac{R}{2})} + t_2 \begin{pmatrix} u \\ i\alpha_2^{-1}u \\ i\alpha_2^{-1}v \\ -v \end{pmatrix} e^{ik_{\downarrow x}^e(x+\frac{R}{2})} + f_1 \begin{pmatrix} i\alpha_1 v \\ v \\ u \\ -i\alpha_1 u \end{pmatrix} e^{-ik_{\uparrow x}^h(x+\frac{R}{2})} + f_2 \begin{pmatrix} i\alpha_2 v \\ -v \\ u \\ i\alpha_2 u \end{pmatrix} e^{-ik_{\downarrow x}^h(x+\frac{R}{2})} \end{aligned} \right\} e^{-(x+\frac{R}{2})/\xi} \\ &+ \left\{ \begin{aligned} &g_1 \begin{pmatrix} u \\ -i\alpha_1^{-1}u \\ i\alpha_1^{-1}v \\ v \end{pmatrix} e^{-ik_{\uparrow x}^e(x+\frac{R}{2})} + g_2 \begin{pmatrix} u \\ i\alpha_2^{-1}u \\ i\alpha_2^{-1}v \\ -v \end{pmatrix} e^{-ik_{\downarrow x}^e(x+\frac{R}{2})} + h_1 \begin{pmatrix} i\alpha_1 v \\ v \\ u \\ -i\alpha_1 u \end{pmatrix} e^{ik_{\uparrow x}^h(x+\frac{R}{2})} + h_2 \begin{pmatrix} i\alpha_2 v \\ -v \\ u \\ i\alpha_2 u \end{pmatrix} e^{ik_{\downarrow x}^h(x+\frac{R}{2})} \end{aligned} \right\} e^{(x-\frac{R}{2})/\xi} \\ &\times \text{for } -\frac{R}{2} < x < \frac{R}{2}, \\ \psi_{N_2}(x) &= e^{ik_y y} \left[c_1 \begin{pmatrix} 1 \\ 0 \\ 0 \\ 0 \end{pmatrix} e^{ik_x(x-\frac{R}{2})} + c_2 \begin{pmatrix} 1 \\ 0 \\ 0 \\ 0 \end{pmatrix} e^{ik_x(x-\frac{R}{2})} + d_1 \begin{pmatrix} 0 \\ 0 \\ 1 \\ 0 \end{pmatrix} e^{-ik_x(x-\frac{R}{2})} + d_2 \begin{pmatrix} 0 \\ 0 \\ 0 \\ 1 \end{pmatrix} e^{-ik_x(x-\frac{R}{2})} \right] \quad \text{for } x > \frac{R}{2}, \end{aligned} \quad (11)$$

with coherence factors for electron (hole) quasiparticles given by $u(v) = \sqrt{(E + (-)\sqrt{E - |\Delta|^2})/2E}$. $\alpha_{1(2)} = k_{\uparrow(\downarrow)}^h/k_{\uparrow(\downarrow)}$ where $k_{\uparrow(\downarrow)} = +(-)(m\lambda/\hbar^2) + \sqrt{(m\lambda/\hbar^2)^2 + k_F^2}$, $k_{\uparrow(\downarrow)}^e = k_{\uparrow(\downarrow)} e^{i\theta_{\uparrow(\downarrow)}}$, and $k_{\uparrow(\downarrow)}^h = k_{\uparrow(\downarrow)} e^{-i\theta_{\uparrow(\downarrow)}}$. $\theta_{\uparrow(\downarrow)}$ denotes phase of the wave with wave number $k_{\uparrow(\downarrow)}$ (see Ref. [22]). As translational symmetry is preserved for the y direction, $k_y = k_F \sin \theta = k_{\uparrow} \sin \theta_{\uparrow} = k_{\downarrow} \sin \theta_{\downarrow}$. $k_{\uparrow(\downarrow)x}^{e(h)}$ denotes the x component of wave vector $k_{\uparrow(\downarrow)x}^{e(h)}$ and is defined as $k_{\uparrow(\downarrow)x}^{e(h)} = \sqrt{(k_{\uparrow(\downarrow)}^{e(h)})^2 - (k_y)^2}$. $a_{1(2)}$ and $b_{1(2)}$ represent scattering amplitudes for Andreev reflection and normal reflection of spin-up (-down) quasiparticles. $c_{1(2)}$ and $d_{1(2)}$ represent scattering amplitudes for elastic cotunneling and cross Andreev reflection of spin-up (-down) quasiparticles. Superconducting coherence length $\xi = \hbar v_F / \Delta$ where v_F is the Fermi velocity [39].

1. Boundary conditions

For pairing symmetries, $p_x\hat{x}$, $p_x\hat{y}$, and helical p (that do not possess spin-rotation symmetry, and are not spin polarized, i.e., \mathbf{d} is not in one fixed spin direction but in both x and y directions, this results in finite diagonal terms in

pairing-potential matrix $\hat{\Delta}$. The scattering amplitudes are determined via the continuity equation and current conservation, which leads to boundary conditions as in Eq. (12) (see also Ref. [37]). The general boundary conditions at the interfaces for US without spin-rotation symmetry, for a $N_1/I/US/I/N_2$ junction at $x = -R/2$ and $R/2$, are given by

$$\begin{aligned} \Psi_{N_1}|_{x=-R/2} &= \Psi_{US}|_{x=-R/2}, & \Psi_{US}|_{x=R/2} &= \Psi_{N_2}|_{x=R/2}, \\ \hbar v_{USx} \Psi_{US}|_{x=-R/2} - \hbar v_{Nx} \Psi_{N_1}|_{x=-R/2} &= -2iU(x)\tau_3 \Psi_{US}|_{x=-R/2}, \\ \hbar v_{Nx} \Psi_{N_2}|_{x=R/2} - \hbar v_{USx} \Psi_{US}|_{x=R/2} &= -2iU(x)\tau_3 \Psi_{US}|_{x=R/2}, \end{aligned} \quad (12)$$

where velocity operator in the x direction [22] is defined by $\hbar v_{USx} = \partial H / \partial k_x$ for US and $\hbar v_{Nx} = \partial H_N / \partial k_x$ where the Hamiltonian H_N for both normal metals N_1 and N_2 is given by setting the pairing potential $\hat{\Delta}(\mathbf{k}) = 0$ in Eq. (10) and diagonal matrix τ_3 is given by $\text{diag}(1, 1, -1, -1)$.

V. RESULTS AND DISCUSSION

Herein, we calculate differential nonlocal conductance G_{NL} , differential shot-noise cross correlations, as well as

shot-noise cross correlations for the 2D $N_1/I/US/I/N_2$ setup as shown in Fig. 2 (see [40] for detailed calculations). We take two cases for bias voltages applied in N_1 and N_2 , i.e., $V_1 = V_2$ (symmetric setup) and $V_1 \neq 0, V_2 = 0$ (nonlocal setup). We plot nonlocal conductance [41,42] and differential shot noise with the propagating phase $k_F R = 55$ and length of the superconductor in terms of superconducting coherence length $R/\xi = 2$. We take these values for propagating phase $k_F R$ and the superconductor's length because when $R \gg \xi$, there will be no possibility of nonlocal transport as electronlike or holelike quasiparticles. These cannot transmit to the normal metal N_2 , and when $R \ll \xi$, the effect of US will be suppressed. However, when the length of superconductor R is comparable to superconducting coherence length ξ , incident quasiparticles can transmit to normal metal N_2 as an electron (EC) or hole (CAR). From Refs. [43,44], one sees a wide range for the propagating phase ($k_F R = 10\text{--}5000$). It has also been shown that nonlocal transport will be suppressed for small values [45] of $k_F R$. In spin-triplet topological superconductor (Sr_2RuO_4) [46], superconducting coherence length $\xi = 91$ nm and superconducting gap $\Delta = 1.76 k_B T_c$, where k_B is Boltzmann constant and critical temperature $T_c = 1.6$ K. Thus, we get a value for Fermi wave vector $k_F = 3 \times 10^8 \text{ m}^{-1}$. In this paper, we take the length of US, $R = 2\xi$. This gives us a value for the propagating phase, i.e., $k_F R \simeq 55$. Hence, in this paper, we take $k_F R$ to be 55. For pairing symmetries without spin-rotational symmetry, i.e., $p_x \hat{x}$, $p_x \hat{y}$, and helical p , we have considered $2m\lambda/\hbar^2 = 0.1k_F$ as has also been taken in Ref. [22]. Substituting the value of k_F , m the mass of electron and \hbar , we get $\lambda = 0.17 \times 10^{-30} \text{ m}$. This λ value corresponds to $2m\lambda/\hbar^2 = 0.1k_F$, implying normalized Rashba spin-orbit strength is around 0.1 times the Fermi wave vector k_F . The next subsection provides results for differential nonlocal conductance and shot-noise cross correlations for different pairing symmetries.

A. Differential nonlocal conductance and differential shot-noise cross correlations

In Fig. 3 we plot differential nonlocal conductance G_{NL} vs bias voltage (eV_1) with $eV_2/\Delta = 0.0$ for intermediate barrier strength ($z = 1$). G_{NL} , dominated by EC, is fully negative for entire range of bias voltage ($-1 < eV_1/\Delta < 1$) irrespective of change in pairing potential for different pairing symmetries. In Appendix A, we describe the crossed Andreev conductance (G_{CAR}) and elastic cotunneling (G_{EC}) contribution to differential nonlocal conductance for each pairing symmetry in the nonlocal setup.

Theoretically, it has been shown that for transparent limit, nonlocal conductance [35,47] is negative, which does not convey enough information about Cooper-pair splitting, known as CAR. It motivates us to study shot-noise cross correlations to differentiate between different pairing symmetries.

Next, let us first look at differential shot-noise cross-correlation behavior for different pairing symmetries due to changes in barrier strength. First, for symmetric setup ($eV_1/\Delta = eV_2/\Delta = 0.2$) as shown in Fig. 4. Differential shot-noise cross correlations (dS^{12}/dV) for helical- p pairing changes sign with increase in barrier strength (z). Positive dS^{12}/dV in case helical- p pairing indicates Cooper-pair split-

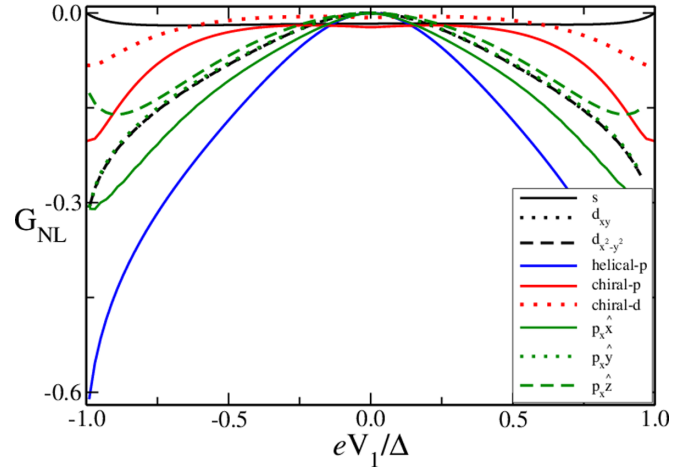


FIG. 3. Differential nonlocal conductance [G_{NL} , see Eq. (3)] in units of $2e^2/h$, for $N_1/I/US/I/N_2$ junction vs bias voltage (eV_1/Δ) for US with different pairing symmetries where $k_F R = 55$, $R/\xi = 2$, $z = 1$, and $eV_2/\Delta = 0$.

ting seen in tunneling regime ($z > 2$), which we explain in detail in the next section. dS^{12}/dV is enhanced in the fully transparent ($z \rightarrow 0$) limit for gapful nontopological s -wave and gapful topological chiral pairings, while it vanishes in tunneling regime ($z \rightarrow \text{large}$). In the transparent limit, dS^{12}/dV slowly increases with increase in barrier strength for nontopological nodal singlet pairing (d_{xy} and $d_{x^2-y^2}$). Increase in barrier strength enhances dS^{12}/dV for topological nodal triplet pairing ($p_x \hat{x}$ and $p_x \hat{y}$). dS^{12}/dV is negative in the transparent limit for nontopological nodal triplet pairing ($p_x \hat{z}$) and vanishes in the tunneling regime.

In Fig. 5 we plot dS^{12}/dV vs z for nonlocal setup with $eV_1/\Delta = 0.2$ and $eV_2/\Delta = 0.0$. Similar results as symmetric setup are obtained for gapful s , chiral pairing, and nodal $p_x \hat{z}$ pairings in nonlocal setup. Unlike symmetric setup, dS^{12}/dV is enhanced in the case of nonlocal setup for topological nodal pairings in the transparent limit. dS^{12}/dV for helical- p pairing

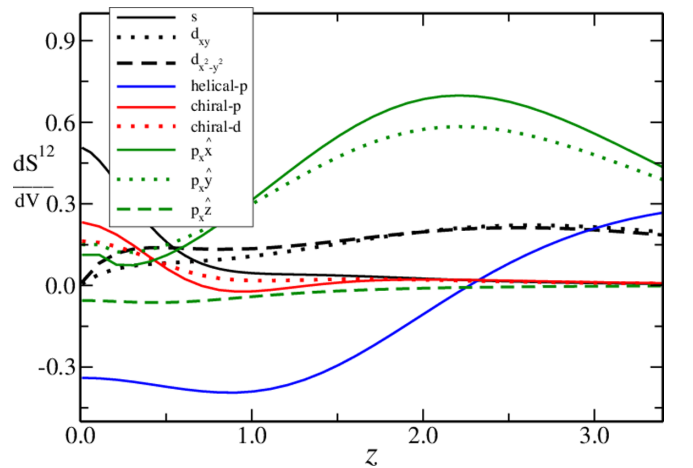


FIG. 4. Differential shot-noise cross correlations [symmetric setup, see Eq. (5)] in units of $4|e|^3/h$ for $N_1/I/US/I/N_2$ junction vs barrier strength (z), with different pairing symmetries where $k_F R = 55$, $R/\xi = 2$, $eV_1/\Delta = eV_2/\Delta = 0.2$.

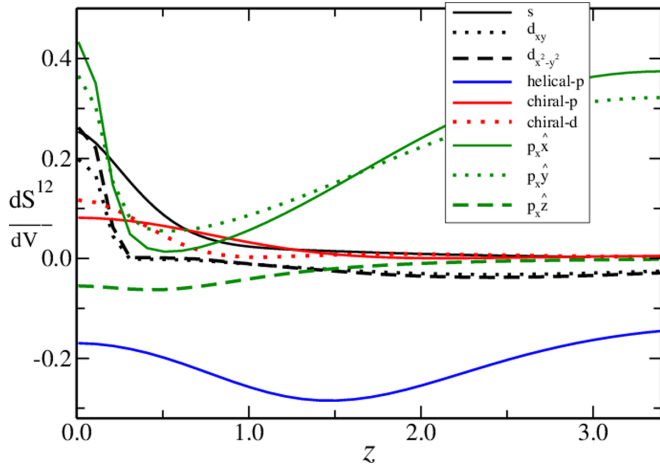


FIG. 5. Differential shot-noise cross correlations [nonlocal setup, see Eq. (6)] in units of $4|e|^3/h$ for $N_1/I/US/I/N_2$ junction vs barrier strength (z) for different pairing symmetries of the unconventional superconductor, with $k_F R = 55$, $R/\xi = 2$, $eV_1/\Delta = 0.2$, and $eV_2/\Delta = 0$.

changes from negative to positive as one goes from transparent to tunneling regime in symmetric setup, while for nonlocal setup, it is completely negative. The opposite behavior is seen for d_{xy} and $d_{x^2-y^2}$ pairing as dS^{12}/dV is completely positive for symmetric setup. However, it changes from positive to negative as one goes from transparent to tunneling regime in a nonlocal setup. For other cases, dS^{12}/dV is always positive for both symmetric and nonlocal setups. Differential shot-noise cross correlations can be a good indicator for helical- p , $p_x\hat{x}$, d_{xy} , and $d_{x^2-y^2}$ pairings.

Next, in Fig. 6 we plot dS^{12}/dV for different pairing symmetries as a function of bias voltage (eV_1/Δ) in the symmetric setup for intermediate barrier strength ($z = 1$). dS^{12}/dV shows zero-bias peak (ZBP) for both nodal nontopological d_{xy} and $d_{x^2-y^2}$ and nodal topological $p_x\hat{x}$ and $p_x\hat{y}$

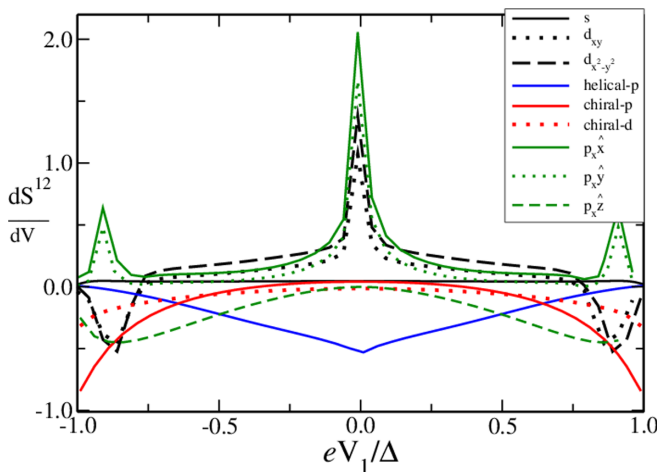


FIG. 6. Differential shot-noise cross correlations (for symmetric setup) in units of $4|e|^3/h$ for $N_1/I/US/I/N_2$ junction vs bias voltage (eV_1/Δ) for different pairing symmetries of the unconventional superconductor, with $k_F R = 55$, $R/\xi = 2$, $eV_1 = eV_2$, and $z = 1$.

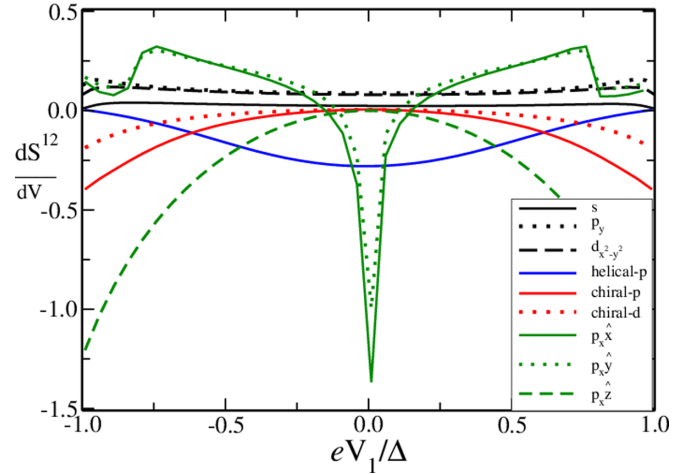


FIG. 7. Differential shot-noise cross correlations (for nonlocal setup) in units of $4|e|^3/h$ for $N_1/I/US/I/N_2$ junction vs bias voltage (eV_1/Δ) for different pairing symmetries with $k_F R = 55$, $R/\xi = 2$, $eV_2/\Delta = 0$, and $z = 1$.

pairings. dS^{12}/dV for gapful topological pairings (helical p , chiral p , and chiral d) and nontopological triplet $p_x\hat{z}$ pairing are negative for the entire range of bias voltage. dS^{12}/dV shows a zero-bias dip (ZBD) for helical p , while it vanishes for chiral- p pairing at zero bias. When bias voltages tend to superconducting gap $\pm\Delta$, dS^{12}/dV is strongly enhanced for chiral pairings.

Next, we plot dS^{12}/dV vs bias voltage (eV_1/Δ) for nonlocal setup with $eV_2/\Delta = 0.0$ in Fig. 7. Tuning the bias voltage eV_2/Δ to zero does not affect dS^{12}/dV for gapful topological pairing (chiral p , chiral d , and helical p) which show similar behavior as in the symmetric setup, shown in Fig. 6. Contrary to symmetric setup, in case of nonlocal setup for nodal topological pairing ($p_x\hat{x}$, $p_x\hat{y}$) dS^{12}/dV shows ZBD instead of ZBP. Table IV summarizes the results for non-local conductance and differential shot noise (in both symmetric and non-local setups). Table IV succinctly puts all results in perspective. In the next subsection, we plot HBT or shot-noise cross correlations in the tunneling and transparent regimes.

B. Shot-noise cross correlations

Shot-noise cross correlations S^{12} for the setup (Fig. 2) in the general case (neither symmetric nor nonlocal) are calculated using Eq. (4) and plotted as function of bias voltage eV_2/Δ applied to normal metal N_2 for both transparent ($z = 0.1$) junction (see Fig. 8) and for tunnel limit ($z = 3$) in Fig. 9. Shot-noise cross correlations for s wave comes in line with previous results [31] for both tunnel and transparent limits.

In Fig. 8, for superconductors that do not possess spin-rotation symmetry, i.e., for gapful helical- p , nodal $p_x\hat{x}$ and $p_x\hat{y}$ cases, shot-noise cross correlations (S^{12}) are negative with a dip at zero bias in the transparent limit. Positive HBT correlations are seen in the transparent limit for superconductors with spin-rotation symmetry. S^{12} for topological chiral- p and chiral- d pairings shows a ZBP and is symmetric as function of bias voltage, whereas S^{12} for all nontopological pairings, i.e., s -wave, $p_x\hat{z}$, d_{xy} , and $d_{x^2-y^2}$, show asymmetric behavior as

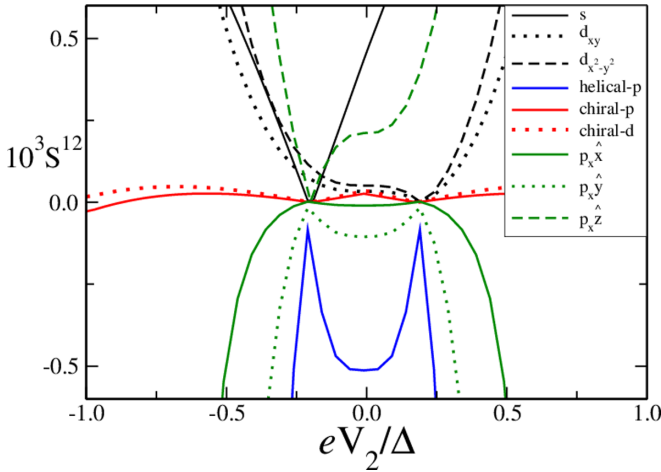


FIG. 8. Shot-noise cross correlations (S^{12} multiplied by 10^3) in units of $4|e|^2/h$ for $N_1/I/US/I/N_2$ junction vs bias voltage (eV_2/Δ) for different pairing symmetries with $k_F R = 55$, $R/\xi = 2$, $eV_1/\Delta = 0.2$, and $z = 0.1$ (transparent barriers).

function of bias voltage V_2 , vanishing at $V_2 = -V_1$ for s wave and $p_x \hat{z}$ and at $V_2 = V_1$ for d_{xy} and $d_{x^2-y^2}$ pairings. Hence, by tuning bias voltages, we can control transport; for example, in the case of topological pairings, there is no transport for both $V_2 = \pm V_1$ whereas for nontopological pairings either at $V_2 = -V_1$ or at $V_2 = V_1$.

In the tunnel limit (Fig. 9), positive shot-noise cross correlations for chiral- p and chiral- d pairings show similar behavior with a ZBP as in the transparent limit. However, contrary to the transparent limit, S^{12} for helical- p pairing in the tunnel limit vanishes at zero bias. Shot-noise cross correlations for s -wave pairing linearly increase as a function of V_2 . Similar to transparent limit, in the tunnel limit S^{12} for all nontopological cases are asymmetric as function of bias voltage and vanish a particular one bias voltage (either $V_2 = V_1$ or $V_2 = -V_1$), whereas for all topological cases S^{12} vanishes at both $V_2 = V_1$ and $V_2 = -V_1$, and is symmetric. Negative

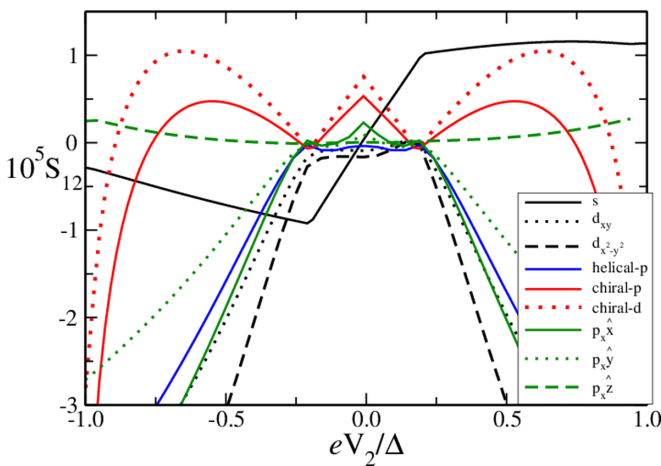


FIG. 9. Shot-noise cross correlations (S^{12} multiplied by 10^5) in units of $4|e|^2/h$ for $N_1/I/US/I/N_2$ junction vs bias voltage (eV_2/Δ) for different pairing symmetries with $k_F R = 55$, $R/\xi = 2$, $eV_1/\Delta = 0.2$, and $z = 3$ (tunnel barriers).

shot-noise cross correlations are seen for nodal nontopological singlet (d_{xy} , $d_{x^2-y^2}$) pairings which vanish at $V_2 = V_1$. At zero bias, S^{12} shows ZBP for topological $p_x \hat{x}$ and $p_x \hat{y}$ whereas it is flat at zero bias for nontopological $p_x \hat{z}$, enabling a distinction between the topological and nontopological p_x pairings. Table V summarizes the results for shot-noise cross correlations in both transparent and tunnel limits.

C. Processes in play

Shot-noise cross correlations have been calculated in metal/superconductor/metal hybrid junctions to study Cooper-pair splitting; see Refs. [35,42,48]. Shot-noise cross correlations for s -wave superconductor show linear behavior, which is $\propto V_2$ in tunnel limit and $\propto eV_1 + eV_2$ in transparent limit for bias voltage range ($-V_1 < V_2 < V_1$) as seen in Figs. 8 and 9. This has been also predicted in Refs. [42,48,49], and explained in Ref. [35]. Shot-noise cross correlations for s -wave pairing vanish at $V_2 = -V_1$ in transparent limit but vanish at $V_2 = 0$ in tunnel limit, which was also predicted in Ref. [49]. One understands this behavior by dividing the shot-noise correlations into individual contributions to shot noise from local (either Andreev reflection or normal reflection) processes and nonlocal (CAR or EC) processes. In the subsections below, we try to understand the reasons for the plots shown in Figs. 8 (transparent limit) and 9 (tunnel limit) for HBT correlations via these processes for all pairing symmetries.

1. Tunnel limit

Shot-noise cross correlations, from Eq. (B1), consist of local [AR (Andreev reflection), NR (normal reflection)] amplitudes and nonlocal [CAR (crossed Andreev reflection), EC (elastic cotunneling)] amplitudes. Each term in the shot-noise cross correlations (B1) consists of four processes which can be grouped as EC-NR, CAR-NR, EC-AR, CAR-AR, and a mixed group of all four processes. EC-NR implies product of elastic cotunneling and normal reflection amplitudes, such as $s_{12}^{ee} s_{21}^{ee} s_{22}^{ee*} s_{11}^{ee*}$; similarly CAR-NR is product of crossed Andreev reflection and normal reflection amplitudes, such as $s_{21}^{eh} s_{12}^{he} s_{11}^{hh*} s_{22}^{ee*}$; CAR-AR is product of crossed Andreev reflection and Andreev reflection amplitudes, such as $s_{21}^{he} s_{12}^{eh} s_{11}^{he*} s_{22}^{eh*}$, and EC-AR is product of elastic cotunneling and Andreev reflection amplitudes, such as $s_{21}^{he} s_{12}^{eh} s_{11}^{he*} s_{22}^{eh*}$.

Inspecting the different contributions for s -wave case, we see that NR amplitudes (s_{11}^{hh} , s_{22}^{ee}) $\rightarrow 1$ in tunnel limit, i.e., large z , hence, CAR-NR terms in S^{12} [see Eq. (B1)] reduce to just CAR (or $s_{CAR} = s_{21}^{eh} s_{12}^{he}$) and EC-NR reduces to just EC (or $s_{EC} = s_{12}^{ee} s_{21}^{ee}$). EC contribution to shot-noise cross correlations in tunnel limit, using electron-hole symmetry of scattering matrix amplitudes, gives $S^{EC} = s_{EC}(h_1 + h_2)$. Here h_1, h_2 are Heaviside theta functions and given in Eq. (B2), while CAR contribution to shot-noise cross correlations in tunnel limit, which again using electron-hole symmetry gives $S^{CAR} = s_{CAR}(h_3 + h_4)$, where h_3, h_4 are given in Eq. (B2). Shot-noise cross correlations for s -wave case in tunnel limit in small-bias voltage regime ($-V_1 < V_2 < V_1$) can be written as $S^{12} = S^{CAR} + S^{EC}$, with $S^{EC} = s_{12}^{ee} s_{21}^{ee} [\Theta(e|V_1 - E) - \Theta(|e|V_2 - E) - \Theta(-|e|V_1 - E) + \Theta(-|e|V_2 - E)]$ and $S^{CAR} = s_{21}^{eh} s_{12}^{he} [-\Theta(e|V_1 - E) -$

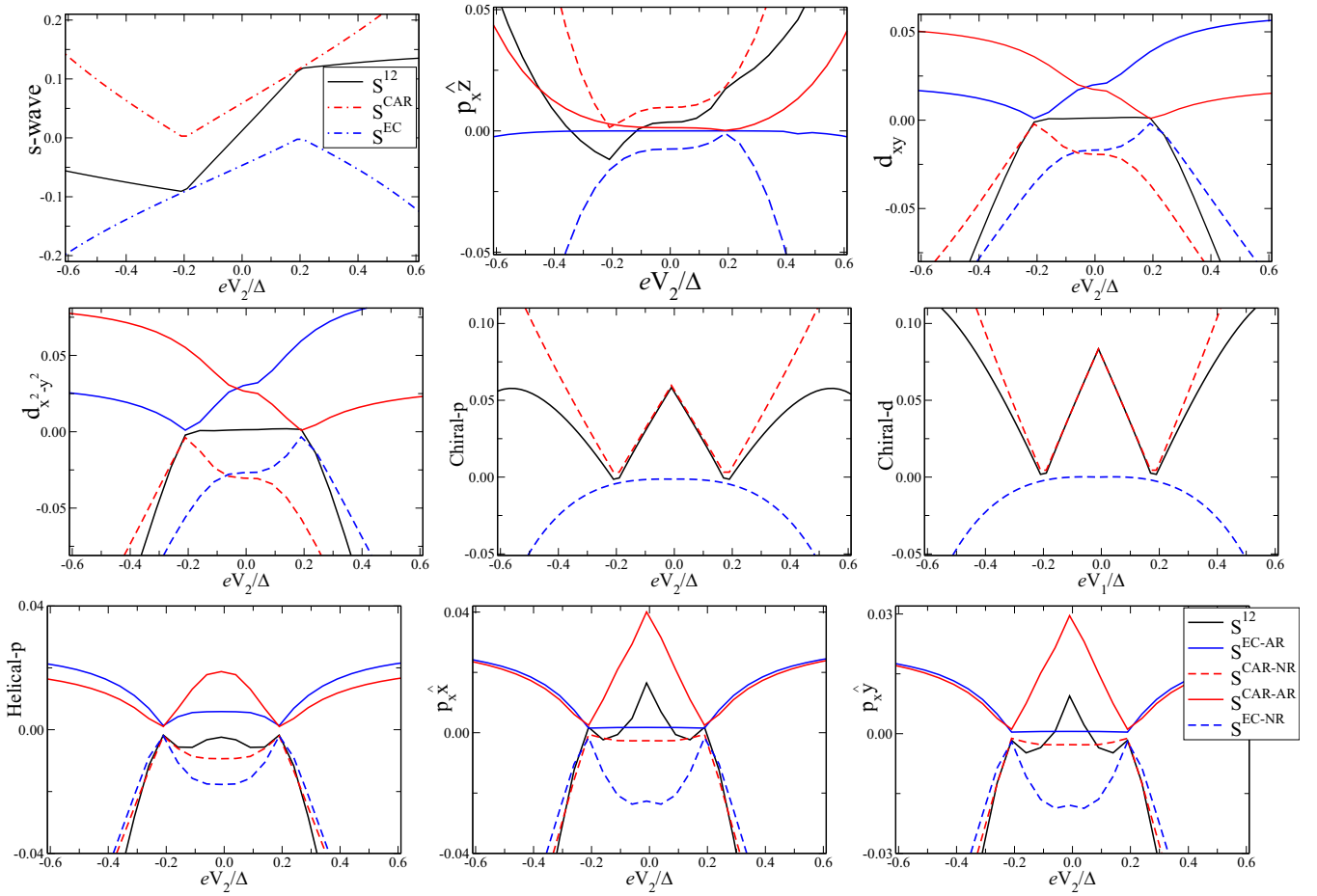


FIG. 10. Processes contributing to shot-noise cross correlations in units of $(10^4) 4|e|^2/h$ for $N_1/I/US/I/N_2$ junction vs bias voltage (eV_2/Δ) for nontopological and topological superconductors with $k_F R = 55$, $R/\xi = 2$, $eV_1/\Delta = 0.2$, $z = 3$ (tunnel barriers).

$\Theta(|e|V_2 - E) + \Theta(-|e|V_1 - E) + \Theta(-|e|V_2 - E)$, where Θ is the Heaviside theta function. However, for other pairing symmetries, NR amplitudes $(s_{11}^{hh}, s_{22}^{ee}) \neq 1$ in tunnel limit. Thus, $S^{\text{CAR-NR}}$ does not reduce to S^{CAR} , and $S^{\text{EC-NR}}$ does not reduce to S^{EC} for these cases. For example, in case of chiral- p , chiral- d , and $p_x \hat{z}$ pairings, $S^{12} = S^{\text{CAR-NR}} + S^{\text{EC-NR}}$, where $S^{\text{CAR-NR}} = (s_{21}^{eh}, s_{12}^{he}, s_{11}^{hh*}, s_{22}^{ee*})(h_3 + h_4)$ and $S^{\text{EC-NR}} = (s_{12}^{ee}, s_{21}^{ee}, s_{22}^{ee*}, s_{11}^{ee*})(h_1 + h_2)$.

From Fig. 10, unlike s -wave (nontopological gapful), shot-noise cross correlations for chiral- p and chiral- d (topological gapful) pairings in tunnel limit are exclusively due to the CAR-NR process at low-bias voltages as EC-NR is suppressed in this regime.

In Fig. 10, essential processes contributing to S^{12} are CAR-NR, CAR-AR, EC-NR, and EC-AR, which vanish at $V_2 = V_1$ or $V_2 = -V_1$ or both $V_2 = \pm V_1$ resulting in no transport at these values for all cases. For chiral (both p and d) superconductors, CAR-NR and EC-NR contribute to HBT correlations. However, EC-NR contribution to HBT correlations vanish at low-bias voltages but dominates at $eV_2 \rightarrow \Delta$, which leads to a change in sign from positive to negative of shot-noise cross correlations. Flat S^{12} is seen at zero bias for $p_x \hat{z}$ pairing due to the contribution of both EC-NR and CAR-NR.

It has been before predicted for s -wave pairing, in Ref. [48], shot-noise cross-correlations in our calculation for

nontopological s -wave superconductor in the tunnel limit in low-bias voltage range $(-V_1 < V_2 < V_1)$ can be written as

$$S_{\text{tunnel}}^{12}(s) \propto eV_2. \quad (13)$$

Similarly S^{12} , in tunnel limit, for gapful topological (chiral p , chiral d , helical p), nodal topological ($p_x \hat{x}$, $p_x \hat{y}$), nodal nontopological superconductors ($p_x \hat{z}$, d_{xy} , $d_{x^2-y^2}$) in low-bias voltage range $(-V_1 < V_2 < V_1)$, one gets

$$S_{\text{tunnel}}^{12}(p_x \hat{z}) \propto (eV_2 + eV_1)^2 - c,$$

$$S_{\text{tunnel}}^{12}(d_{xy}, d_{x^2-y^2}) \propto -(c eV_2 - eV_1)^2,$$

$$S_{\text{tunnel}}^{12}(\text{chiral } p \text{ and chiral } d) \propto (eV_1 - |eV_2|),$$

$$S_{\text{tunnel}}^{12}(\text{helical } p) \propto -[eV_1 |eV_2| - (eV_2)^2],$$

$$S_{\text{tunnel}}^{12}(p_x \hat{x}, p_x \hat{y}) \propto (-|eV_2| + c eV_1) - |(eV_2)^2 - (eV_1)^2|, \quad (14)$$

where c is a constant term. For topological superconductors, S^{12} in tunnel limit is symmetric to change in sign of bias voltage (V_2), whereas for nontopological superconductors, it is asymmetric as a function of bias voltage (V_2). This symmetry can be a marker also for the presence of Majorana fermions akin to ZBCP in metal and topological superconductor junction. Shot-noise cross correlations predicted in our work for s

TABLE II. Processes that contribute to shot-noise cross correlations are denoted by \checkmark and \times represents the processes that do not contribute to shot-noise cross correlations at a low-bias voltage range ($-V_1 < V_2 < V_1$) for each pairing in the tunnel limit.

Topology	Type	Pairing	EC-AR	CAR-AR	EC-NR	CAR-NR
			$(\langle \Delta I_{N_1}^e \Delta I_{N_2}^e \rangle + \langle \Delta I_{N_1}^h \Delta I_{N_2}^e \rangle)$	$(\langle \Delta I_{N_1}^e \Delta I_{N_2}^e \rangle + \langle \Delta I_{N_1}^h \Delta I_{N_2}^h \rangle)$	$(\langle \Delta I_{N_1}^e \Delta I_{N_2}^e \rangle + \langle \Delta I_{N_1}^h \Delta I_{N_2}^h \rangle)$	$(\langle \Delta I_{N_1}^e \Delta I_{N_2}^e \rangle + \langle \Delta I_{N_1}^h \Delta I_{N_2}^e \rangle)$
Nontopological	Gapful	s	\times	\times	\checkmark	\checkmark
	Nodal	$p_x \hat{z}$	\times	\times	\checkmark	\checkmark
		$d_{x^2-y^2}, d_{xy}$	\checkmark	\checkmark	\checkmark	\checkmark
Topological	Chiral	$p_x + ip_y$	\times	\times	\checkmark	\times
	(Gapful)	$d_{x^2-y^2} + id_{xy}$				
	Helical	p	\checkmark	\checkmark	\checkmark	\checkmark
	(Gapful)					
	Nodal	$p_x \hat{x}, p_x \hat{y}$	\checkmark	\checkmark	\checkmark	\checkmark

wave are in line with that seen for s -wave superconductor in Refs. [48,49].

Table II summarizes how the different processes contribute to the shot-noise cross correlations as a function of bias voltages. Current is carried by electrons or holes, i.e., I^e or I^h . Shot-noise cross correlations can be categorized based on correlation between same type of carriers, i.e., $\langle \Delta I_{N_1}^e \Delta I_{N_2}^e \rangle + \langle \Delta I_{N_1}^h \Delta I_{N_2}^h \rangle$ for EC-NR and CAR-AR or between different types of carriers, i.e., $\langle \Delta I_{N_1}^e \Delta I_{N_2}^h \rangle + \langle \Delta I_{N_1}^h \Delta I_{N_2}^e \rangle$ for EC-AR and CAR-NR. Hence, EC-AR and CAR-NR behave similarly due to different charge-carrier correlations, e.g., in the case of nontopological d_{xy} and $d_{x^2-y^2}$ pairings, while EC-NR and CAR-AR behave similarly due to correlations between same charge carriers, e.g., in case of helical- p , $p_x \hat{x}$, and $p_x \hat{y}$ pairings which are topological. For nontopological $p_x \hat{z}$ pairing and topological chiral- p and chiral- d pairing, AR contribution tends to be negligible, hence, suppressing EC-AR and CAR-AR contributions at low-bias voltages.

2. Transparent limit

From Ref. [35], for s -wave pairing, shot-noise cross correlations in transparent limit contribute only from the EC-AR process. Along with s -wave, shot-noise cross correlations for chiral- p , chiral- d , and $p_x \hat{z}$ pairings in transparent limit ($z = 0.0$) are limited to EC-AR, as CAR-NR contribution is negligible. Thus, for s -wave, chiral- p , chiral- d , and $p_x \hat{z}$ pairings, $S^{12} = S^{\text{EC-AR}} = s_{\text{EC-AR}} h_{\text{EC-AR}}$, where $s_{\text{EC-AR}} = s_{12}^{ee} s_{21}^{hh} s_{11}^{eh*} s_{22}^{he*}$ and $h_{\text{EC-AR}} = h_3 + h_4$, h_3 and h_4 are Heaviside theta functions given in Eq. (B2). Simplifying the shot-noise cross correlations for s -wave, chiral- p , chiral- d , and $p_x \hat{z}$ pairings in transparent limit ($z = 0.0$), and in low-bias voltage regime $-V_1 < V_2 < V_1$, we get $S^{12} = S^{\text{EC-AR}} = (s_{12}^{ee} s_{21}^{hh} s_{11}^{eh*} s_{22}^{he*}) [-\Theta(e|V_1 - E) - \Theta(|e|V_2 - E) + \Theta(-|e|V_1 - E) + \Theta(-|e|V_2 - E)]$, where Θ is Heaviside theta function. All four processes (EC-AR, EC-NR, CAR-AR, and CAR-NR) contribute to shot-noise cross correlations for superconductors that do not possess spin-rotation symmetry. In contrast, only one process contributes to shot-noise cross correlations for superconductors that possess spin-rotation symmetry in a low-bias voltage range. Hence, for d_{xy} and $d_{x^2-y^2}$ cases, $S^{12} = S^{\text{CAR-AR}}$ at low-bias voltages. CAR-AR contribution to shot noise can be written as $S^{\text{CAR-AR}} = s_{\text{CAR-AR}} h_{\text{CAR-AR}}$, where $s_{\text{CAR-AR}} = s_{21}^{eh} s_{12}^{he} s_{11}^{he*} s_{22}^{eh*}$

and $h_{\text{CAR-AR}} = h_1 + h_4$, h_1 and h_4 are Heaviside theta functions given in Eq. (B2).

Similar to tunnel limit in the transparent limit, processes that contribute to S^{12} are asymmetric as function of V_2 and lead to no transport at $V_2 = -V_1$ for s -wave case and at $V_2 = V_1$ for d_{xy} and $d_{x^2-y^2}$ cases as given in Eq. (15). For all topological cases, processes that contribute to S^{12} are symmetric as function of V_2 resulting in vanishing S^{12} at both $V_2 = V_1$ and $V_2 = -V_1$ as shown in Fig. 11. Shot-noise cross correlations for all pairing symmetries in Fig. 11 shown for $z = 0.0$ (transparent limit) show similar behavior as also seen in Fig. 8 for $z = 0.1$.

As also predicted in Ref. [49], shot-noise cross correlations for s -wave superconductor in transparent limit at zero temperature reduces to

$$S_{\text{transparent}}^{12}(s) \propto eV_1 + eV_2. \quad (15)$$

In the transparent limit and low-bias voltage range ($-V_1 < V_2 < V_1$), shot-noise cross correlations for the rest of the pairing symmetries are given as

$$\begin{aligned} S_{\text{transparent}}^{12}(\text{chiral } p, \text{ chiral } d) &\propto eV_1 - |eV_2|, \\ S_{\text{transparent}}^{12}(p_x \hat{z}) &\propto (c eV_2 + eV_1)^2, \\ S_{\text{transparent}}^{12}(d_{xy}, d_{x^2-y^2}) &\propto (c eV_2 - eV_1)^2, \\ S_{\text{transparent}}^{12}(\text{helical } p, p_x \hat{x}, p_x \hat{y}) &\propto (eV_2)^2 - (eV_1)^2, \end{aligned} \quad (16)$$

where c is a constant value. Bias-voltage dependence of shot-noise cross correlations for chiral pairing is the same in both transparent and tunnel limits. In contrast, barrier strength influences bias-voltage dependence of shot-noise cross correlations for other cases.

Different processes that contribute to shot-noise cross correlations as a function of bias voltages are summarized in Table III in the low-bias voltage range ($-V_1 < V_2 < V_1$) for transparent limit. All four processes contribute to shot-noise cross correlations for superconductors that do not possess spin-rotation symmetry in 2D. In contrast, for superconductors that possess spin-rotation symmetry, only one process

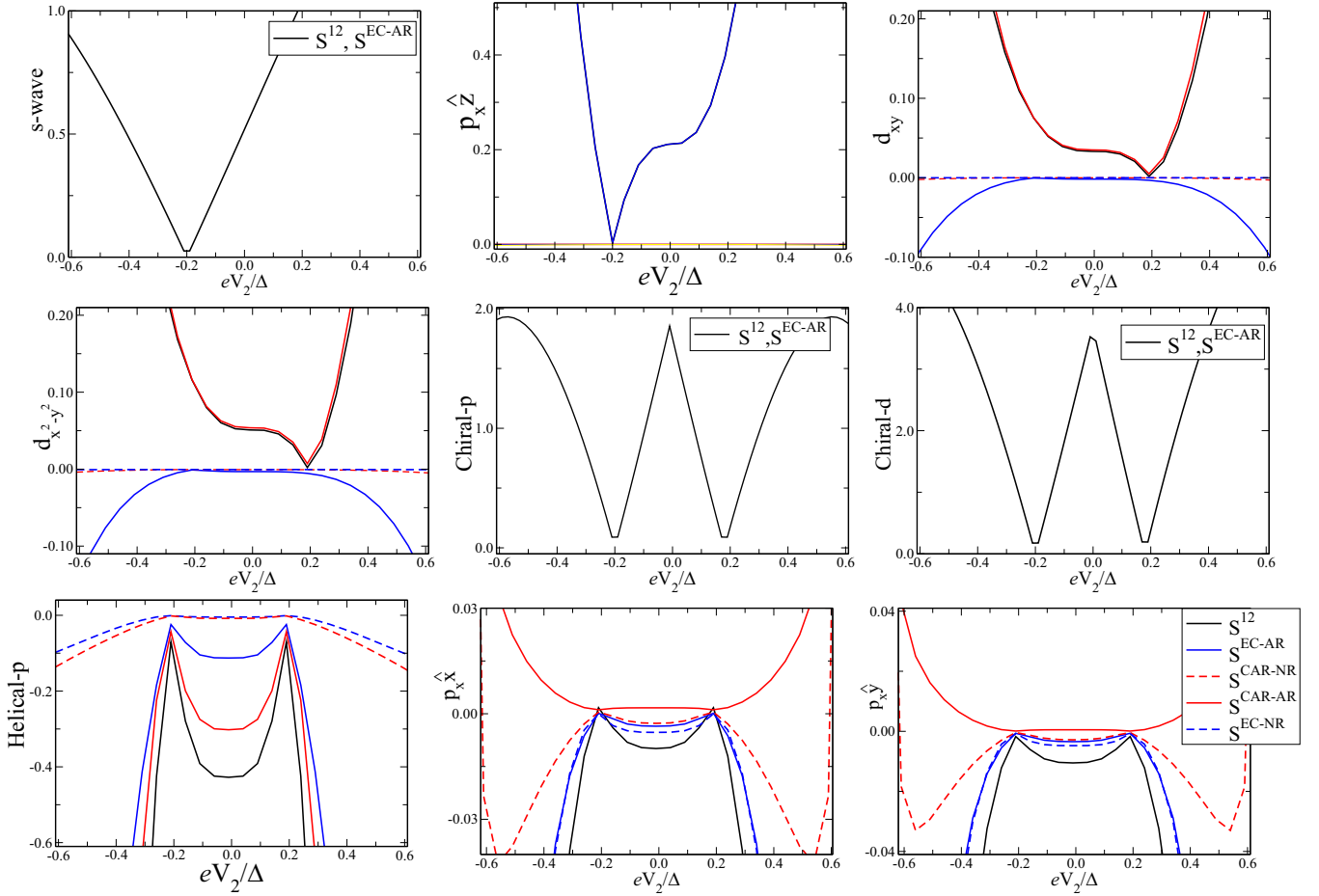


FIG. 11. Processes contributing to shot-noise cross correlations in units of $4|e|^2/h$ for $N_1/I/US/I/N_2$ junction vs bias voltage (eV_2/Δ) for nontopological superconductors $S^{12}(10^3)$ and topological superconductors $S^{12}(10^5)$ with $k_F R = 55$, $R/\xi = 2$, $eV_1/\Delta = 0.2$, and $z = 0.0$ (transparent limit).

contributes to noise cross correlations at low-bias voltages. We have observed that shot-noise cross correlations for unconventional superconductors do not obey the linearity in bias voltage V_2 , like s wave.

VI. EXPERIMENTAL REALIZATION AND CONCLUSION

Experiments on NSN junctions, similar to those shown in Fig. 2, but with s -wave superconductors, are already a decade

old. In Refs. [50,51], positive shot-noise cross correlations were experimentally observed for the first time in a NSN junction with copper being the metal and aluminium as a s -wave superconductor. Next, in Ref. [52], when gold replaced copper as the metal in the NSN junction, similar positive shot-noise cross correlations were again seen. Uniquely, in Ref. [52], the effects of an external magnetic field on shot-noise cross correlations were also taken into account. Finally, in a more recent experiment, shot-noise autocorrelations were

TABLE III. Processes that contribute to shot-noise cross correlations are denoted by \checkmark and \times represents the processes that do not contribute to shot-noise cross correlations at low-bias voltage ($-V_1 < V_2 < V_1$) for each pairing in transparent limit.

Topology	Type	Pairing	EC-AR ($\langle \Delta I_{N_1}^e \Delta I_{N_2}^h \rangle + \langle \Delta I_{N_1}^h \Delta I_{N_2}^e \rangle$)	CAR-AR ($\langle \Delta I_{N_1}^e \Delta I_{N_2}^e \rangle + \langle \Delta I_{N_1}^h \Delta I_{N_2}^h \rangle$)	EC-NR ($\langle \Delta I_{N_1}^e \Delta I_{N_2}^e \rangle + \langle \Delta I_{N_1}^h \Delta I_{N_2}^h \rangle$)	CAR-NR ($\langle \Delta I_{N_1}^e \Delta I_{N_2}^h \rangle + \langle \Delta I_{N_1}^h \Delta I_{N_2}^e \rangle$)
Nontopological	Gapful	s	\checkmark	\times	\times	\times
	Nodal	$p_x \hat{z}$	\checkmark	\times	\times	\times
Topological		$d_{x^2-y^2}, d_{xy}$	\times	\checkmark	\times	\times
	Chiral	$p_x + ip_y$	\checkmark	\times	\times	\times
	(Gapful)	$d_{x^2-y^2} + id_{xy}$	\checkmark	\checkmark	\checkmark	\checkmark
	Helical	p	\checkmark	\checkmark	\checkmark	\checkmark
	(Gapful)		\checkmark	\checkmark	\checkmark	\checkmark
	Nodal	$p_x \hat{x}, p_x \hat{y}$	\checkmark	\checkmark	\checkmark	\checkmark

TABLE IV. Characteristics of differential nonlocal conductance and differential shot-noise cross correlations in $N_1/I/US/I/N_2$ junction.

Topology	Type	Pairing	Differential-shot noise cross correlation										
			Differential nonlocal conductance		Symmetric setup		Nonlocal setup						
			$z = 1, eV_2/\Delta = 0$	$eV_1/\Delta = \pm\Delta$	$z = 1, eV_1 = eV_2$	$eV_1/\Delta = 0$	$eV_1/\Delta = \pm\Delta$	$z = 1, eV_2/\Delta = 0$	$eV_1/\Delta = 0.2$	$eV_2/\Delta = 0$			
Nontopological	Gapful	s	Flat, Negative	Vanishing	Flat, Positive	Vanishing	Flat, Positive	Vanishing	Positive	Vanishing	Positive	Vanishing	
	Nodal	$p_x\hat{z}$	Vanishing	Negative	Vanishing	Positive	Vanishing	Negative	Vanishing	Negative	Vanishing	Negative	Vanishing
		$d_{x^2-y^2}$	Vanishing	Negative	ZBP, Positive	Vanishing	Positive	Vanishing	Positive	Vanishing	Positive	Vanishing	Negative
		d_{xy}	Vanishing	Negative	ZBP, Positive	Vanishing	Positive	Vanishing	Positive	Vanishing	Positive	Vanishing	Negative
Topological	Chiral	$p_x + ip_y$	Flat, Negative	Negative	Flat, Positive	Negative	Vanishing	Negative	Positive	Vanishing	Positive	Vanishing	
	(Gapful)		Flat, Negative	Negative	Flat, Vanishing	Negative	Flat, Vanishing	Negative	Positive	Vanishing	Positive	Vanishing	
	Helical	$d_{x^2-y^2} + id_{xy}$	ZBD, Negative	Vanishing	ZBD, Negative	Vanishing	Vanishing	ZBD, Negative	Vanishing	Negative	Positive	Negative	Vanishing
		p	Vanishing	Negative	ZBP, Positive	Vanishing	Vanishing	ZBD, Negative	Vanishing	Positive	Positive	Negative	Vanishing
Nodal	$p_x\hat{x}$	Vanishing	Negative	ZBP, Positive	Vanishing	Vanishing	ZBD, Negative	Vanishing	Positive	Positive	Positive	Positive	
	$p_x\hat{y}$	Vanishing	Negative	ZBP, Positive	Vanishing	Vanishing	ZBD, Negative	Vanishing	Positive	Positive	Positive	Positive	

TABLE V. Characteristics of shot-noise crosscorrelations in $N_1/I/US/I/N_2$ junction.

		Shot-noise cross correlations ($eV_1/\Delta = 0.2$)								
		$z = 0.1$			$z = 3$					
Topology	Type	Pairing	$eV_2/\Delta \rightarrow 0$	$eV_2 = eV_1$	$eV_2 = -eV_1$	$-eV_1 < eV_2 < eV_1$	$eV_2/\Delta \rightarrow 0$	$eV_2 = eV_1$	$eV_2 = -eV_1$	$-eV_1 < eV_2 < eV_1$
Nontopological	Gapful	s	Positive	Finite, Positive	Vanishing	Vanishing	Vanishing	Positive	Negative	eV_2
	Nodal	$p_x\hat{x}$ $d_{xy}, d_{x^2-y^2}$	Flat, Positive Flat, Positive	Positive Vanishing	Vanishing Positive	Vanishing Positive	Flat, Positive Flat, Negative	Positive Vanishing	Negative Negative	$(eV_2 + eV_1)^2 - c$ $-(c eV_2 - eV_1)^2$
Topological	Chiral (Gapful)	$p_x + ip_y$ $d_{x^2-y^2} + id_{xy}$	ZBP, Positive	Vanishing	Vanishing	Vanishing	ZBP, Positive	Vanishing	Vanishing	$eV_1 - eV_2 $
	Helical (Gapful)	p	Negative	Vanishing	Vanishing	Vanishing	Vanishing	Vanishing	Vanishing	$(eV_2)^2 - (eV_1)^2$
	Nodal	$p_x\hat{x}, p_x\hat{y}$	Negative	Vanishing	Vanishing	Vanishing	ZBP, Positive	Vanishing	Vanishing	$-(eV_2 + c eV_1) - (eV_2)^2 - (eV_1)^2 $

measured in a metal–high- T_c cuprate superconductor junction [53]. Extending these experimental setups to metal-2D unconventional superconductor-metal junctions and measuring shot-noise cross correlations should reveal the signatures of the distinct pairing symmetries. Suggested pairing symmetries for Sr_2RuO_4 are still in conflict but recent anisotropic strain experiment in Sr_2RuO_4 suggests pairing as chiral p [54].

In Table IV, we summarize the results of our work concerning differential nonlocal conductance and differential shot-noise cross correlations in both symmetric and nonlocal setups. Whether we consider symmetric or nonlocal setup, differential shot-noise cross correlations for helical- p superconductor are always negative in the transparent limit. Further, for the entire range of bias voltages, shot noise is negative for helical- p pairing. It is the unique signature of helical- p pairing. In the transparent and tunnel limits, we summarize the results of shot-noise cross correlations in Table V. Irrespective of whether tunnel limit or transparent, HBT correlations for nontopological pairings are always asymmetric to the sign of bias voltage and symmetric for topological pairings.

Our approach using nonlocal differential conductance, differential shot-noise cross correlations, and shot-noise cross correlations to probe chiral (p and d), as well as helical- p and nodal pairing in topological superconductors, will help distinguish helical from chiral and nodal pairing, unlike Knight shift measurement that does not resolve the helical and chiral dichotomy. Our method will give an easy way for experimentalists to distinguish nontopological superconductors from chiral, nodal, as well as helical- p superconductors via differential shot-noise cross correlations and shot-noise cross correlations. We have considered a finite but small value of Rashba spin-orbit coupling λ for cases without spin-rotation symmetry, i.e., $p_x\hat{x}$, $p_x\hat{y}$, and helical p which has a minor effect on the magnitude of the results as compared to that for $\lambda = 0$. In the future, we will extend our study to probe the topological character of superconducting Dirac materials using shot-noise cross correlations.

ACKNOWLEDGMENT

This work was supported by the grants ‘‘Josephson junctions with strained Dirac materials and their application in quantum information processing’’ from Science & Engineering Research Board (SERB), New Delhi, Government of India, under Grant No. CRG/2019/006258.

APPENDIX A: DIFFERENTIAL NONLOCAL CONDUCTANCE

In Fig. 12, we plot G_{CAR} and G_{EC} vs barrier strength (z) for nonlocal setup with $eV_1/\Delta = 0.2$, $eV_2/\Delta = 0.0$. G_{CAR} for helical p superconductor tends to a finite value in the tunnel limit, while for other cases tends to zero. G_{EC} for helical p superconductor tends to a finite value, but G_{EC} for other cases tend to zero in the tunnel limit ($z \rightarrow \text{large}$). G_{NL} is always dominated by G_{EC} . In Fig. 13, we plot G_{NL} vs z in nonlocal setup with $eV_1/\Delta = 0.2$, $eV_2/\Delta = 0.0$. G_{NL} for all pairings tends to zero in the tunnel limit ($z \rightarrow \text{large}$). One does not see any marked difference between topological and

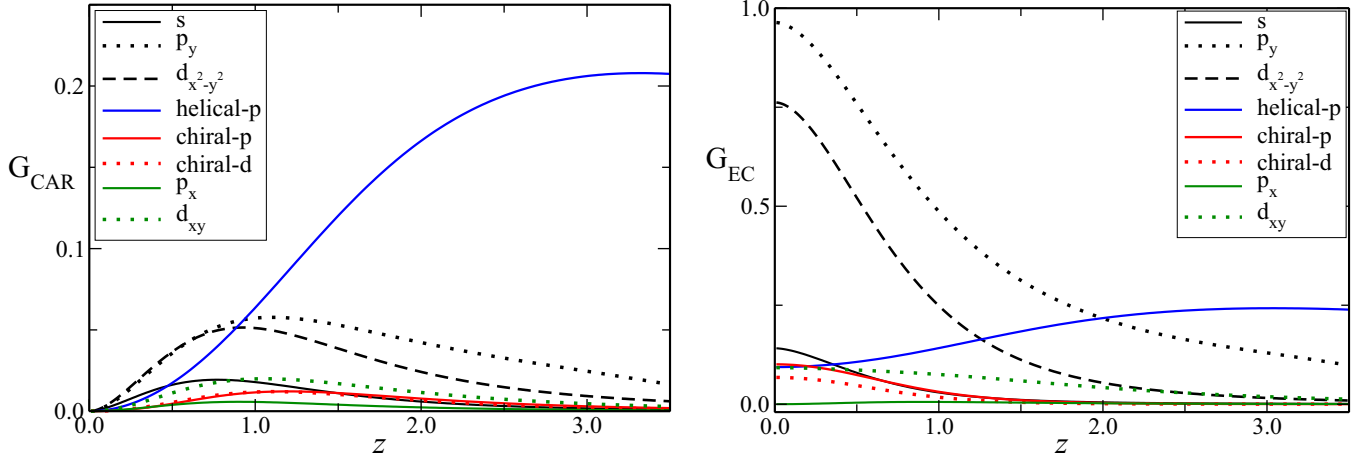


FIG. 12. Crossed Andreev conductance G_{CAR} (left) and elastic cotunneling G_{EC} (right) for $N_1/I/US/I/N_2$ junction vs barrier strength (z) for US with different pairing symmetries with $k_F R = 55$, $R/\xi = 2$, $eV_1/\Delta = 0.2$, and $eV_2/\Delta = 0$.

nontopological superconductors from the nonlocal conductance. It is because the electron cotunneling conductance dominates the crossed Andreev conductance.

APPENDIX B: SHOT-NOISE CROSS CORRELATION

This Appendix expands the shot-noise cross-correlations formula regarding scattering amplitudes. Shot-noise cross correlations as given in Eq. (4) can be expanded as

$$S^{12} = \frac{4e^2}{h} \int_{-\pi/2}^{\pi/2} d\theta \frac{\cos \theta}{2\pi} \int dE \{ (s_1 + s_2)h_1 + (s_3 + s_4)h_2 + (s_5 + s_6)h_3 + (s_7 + s_8)h_4 + s_9h_5 + s_{10}h_6 + s_{11}h_7 + s_{12}h_8 + s_{13}h_9 + s_{14}h_{10} \}. \quad (\text{B1})$$

The Fermi functions as given in Eq. (2) for electron and hole in contact i are $f_{ie}(E) = [1 + \exp(\frac{E - |e|V_i}{k_B T})]^{-1}$ and $f_{ih}(E) = [1 + \exp(\frac{E + |e|V_i}{k_B T})]^{-1}$, where k_B is Boltzmann constant and T is temperature. At zero temperature, $f_{ie}(E) \rightarrow \Theta(|e|V_i - E)$

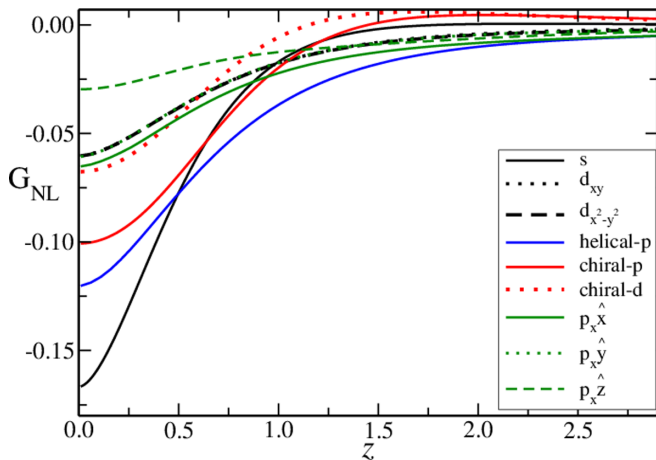


FIG. 13. G_{NL} for $N_1/I/US/I/N_2$ junction vs barrier strength (z) for US with different pairing symmetries where $k_F R = 55$, $R/\xi = 2$, $eV_1/\Delta = 0.2$, and $eV_2/\Delta = 0$.

and $f_{ih}(E) \rightarrow \Theta(|e|V_i + E)$, where Θ is the Heaviside theta function.

The variables s_i to $i = 1, \dots, 14$ and Heaviside theta function components h_i to $i = 1, \dots, 10$ given in Eq. (B1) are

$$\begin{aligned} h_1 &= \Theta(|e|V_1 - E) - 2\Theta(|e|V_1 - E)\Theta(|e|V_2 - E) + \Theta(|e|V_2 - E), \\ h_2 &= \Theta(-|e|V_1 - E) - 2\Theta(-|e|V_1 - E)\Theta(-|e|V_2 - E) + \Theta(-|e|V_2 - E), \\ h_3 &= -\Theta(-|e|V_1 - E) + 2\Theta(-|e|V_1 - E)\Theta(|e|V_2 - E) - \Theta(|e|V_2 - E), \quad h_4 = -\Theta(|e|V_1 - E) \\ &\quad + 2\Theta(|e|V_1 - E)\Theta(-|e|V_2 - E) - \Theta(-|e|V_2 - E), \\ h_5 &= -\Theta(-|e|V_1 - E) + 2\Theta(-|e|V_1 - E)\Theta(-|e|V_2 - E) - \Theta(-|e|V_2 - E), \\ &\quad h_6 = -\Theta(|e|V_1 - E) + 2\Theta(|e|V_1 - E)\Theta(|e|V_2 - E) - \Theta(|e|V_2 - E), \\ h_7 &= \Theta(-|e|V_1 - E) - 2\Theta(-|e|V_1 - E)\Theta(|e|V_2 - E) + \Theta(|e|V_2 - E), \quad h_8 = \Theta(|e|V_1 - E) \\ &\quad - 2\Theta(|e|V_1 - E)\Theta(-|e|V_2 - E) + \Theta(-|e|V_2 - E), \\ h_9 &= \Theta(|e|V_2 - E) - 2\Theta(|e|V_2 - E)\Theta(-|e|V_2 - E) + \Theta(-|e|V_2 - E), \quad h_{10} = \Theta(|e|V_1 - E) \\ &\quad - 2\Theta(|e|V_1 - E)\Theta(-|e|V_1 - E) + \Theta(-|e|V_1 - E), \end{aligned}$$

$$s_1 = \{s_{12}^{ee} s_{11}^{ee*} s_{21}^{ee} s_{22}^{ee*}\}, \quad s_2 = \{s_{21}^{he} s_{11}^{he*} s_{12}^{he} s_{22}^{he*}\},$$

$$s_3 = \{s_{12}^{hh} s_{11}^{hh*} s_{21}^{hh} s_{22}^{hh*}\}, \quad s_4 = \{s_{12}^{eh} s_{11}^{eh*} s_{21}^{eh} s_{22}^{eh*}\},$$

$$s_5 = \{s_{21}^{eh} s_{11}^{eh*} s_{12}^{ee} s_{22}^{ee*}\}, \quad s_6 = \{s_{12}^{ee} s_{11}^{ee*} s_{21}^{he} s_{22}^{he*}\},$$

$$s_7 = \{s_{12}^{eh} s_{11}^{eh*} s_{21}^{he} s_{22}^{he*}\}, \quad s_8 = \{s_{12}^{hh} s_{11}^{hh*} s_{21}^{ee} s_{22}^{ee*}\},$$

$$s_9 = \{s_{12}^{eh} s_{22}^{eh*} s_{21}^{hh} s_{11}^{hh*} + s_{12}^{hh} s_{11}^{hh*} s_{21}^{eh} s_{22}^{eh*}\},$$

$$s_{10} = \{s_{12}^{ee} s_{11}^{ee*} s_{21}^{he} s_{22}^{he*} + s_{21}^{ee} s_{22}^{ee*} s_{12}^{he} s_{11}^{he*}\},$$

$$s_{11} = \{s_{12}^{ee} s_{22}^{ee*} s_{21}^{eh} s_{11}^{eh*} + s_{21}^{hh} s_{11}^{hh*} s_{12}^{he} s_{22}^{he*}\},$$

$$s_{12} = \{s_{12}^{eh} s_{11}^{eh*} s_{21}^{ee} s_{22}^{ee*} + s_{12}^{hh} s_{22}^{hh*} s_{21}^{he} s_{11}^{he*}\},$$

$$\begin{aligned}
 s_{13} &= \{s_{11}^{eh} s_{11}^{ee*} s_{21}^{ee} s_{21}^{eh*} + s_{21}^{hh} s_{11}^{hh*} s_{11}^{he} s_{21}^{he*} \\
 &\quad - s_{11}^{hh} s_{21}^{eh*} s_{21}^{ee} s_{11}^{he*} - s_{11}^{ee} s_{21}^{he*} s_{21}^{hh} s_{11}^{eh*}\}, \\
 s_{14} &= \{s_{12}^{ee} s_{22}^{ee*} s_{12}^{eh} s_{12}^{eh*} + s_{12}^{eh} s_{22}^{hh*} s_{22}^{he} s_{12}^{he*} \\
 &\quad - s_{12}^{eh} s_{12}^{ee*} s_{22}^{he} s_{22}^{hh*} - s_{12}^{hh} s_{12}^{he*} s_{22}^{ee} s_{22}^{eh*}\}.
 \end{aligned} \tag{B2}$$

EC-NR processes are identified by s_1 and s_3 , while CAR-AR processes are s_2 and s_4 . CAR-NR processes are identified by s_5 and s_7 , while EC-AR processes are s_6 and s_8 . Finally, s_9 – s_{14} are identified as mixed processes that consist of scattering amplitudes of all four processes, i.e., EC, CAR, AR, and NR.

- [1] H. R. Ott, H. Rudigier, T. M. Rice, K. Ueda, Z. Fisk, and J. L. Smith, *Phys. Rev. Lett.* **52**, 1915 (1984).
- [2] J.-X. Yin, Z. Wu, J.-H. Wang, Z.-Y. Ye, J. Gong, X.-Y. Hou, L. Shan, A. Li, X.-J. Liang, X.-X. Wu *et al.*, *Nat. Phys.* **11**, 543 (2015).
- [3] A. K. Nayak, A. Steinbok, Y. Roet, J. Koo, G. Margalit, I. Feldman, A. Almoalem, A. Kanigel, G. A. Fiete, B. Yan *et al.*, *Nat. Phys.* **17**, 1413 (2021).
- [4] J. Alicea, *Rep. Prog. Phys.* **75**, 076501 (2012); C. W. J. Beenakker, *Rev. Condens. Matter Phys.* **4**, 113 (2013).
- [5] M. S. Scheurer and J. Schmalian, *Nat. Commun.* **6**, 6005 (2015); S. Das Sarma, C. Nayak, and S. Tewari, *Phys. Rev. B* **73**, 220502(R) (2006).
- [6] A. J. Leggett and Y. Liu, *J. Supercond. Novel Magn.* **34**, 1675 (2021).
- [7] K. Ishida, H. Mukuda, Y. Kitaoka, K. Asayama, Z. Q. Mao, Y. Mori, and Y. Maeno, *Nature (London)* **396**, 658 (1998); A. J. Leggett, *Phys. Rev. Lett.* **14**, 536 (1965); H. Mukuda, K. Ishida, Y. Kitaoka, K. Asayama, Z. Q. Mao, Y. Mori, and Y. Maeno, *J. Phys. Soc. Jpn.* **67**, 3945 (1998).
- [8] S. Kashiwaya, K. Saitoh, H. Kashiwaya, M. Koyanagi, M. Sato, K. Yada, Y. Tanaka, and Y. Maeno, *Phys. Rev. B* **100**, 094530 (2019).
- [9] A. P. Schnyder, S. Ryu, A. Furusaki, and A. W. W. Ludwig, *Phys. Rev. B* **78**, 195125 (2008); C. K. Chiu, J. C. Y. Teo, A. P. Schnyder, and S. Ryu, *Rev. Mod. Phys.* **88**, 035005 (2016).
- [10] P. Burset, F. Keidel, Y. Tanaka, N. Nagaosa, and B. Trauzettel, *Phys. Rev. B* **90**, 085438 (2014).
- [11] S. Matsuo, H. Sugiura, and S. Noguchi, *J. Low Temp. Phys.* **15**, 481 (1974); P. M. Tedrow, R. Meservey, and B. B. Schwartz, *Phys. Rev. Lett.* **24**, 1004 (1970).
- [12] J. R. Kirtley, C. C. Tsuei, J. Z. Sun, C. C. Chi, L. S. Yu-Jahnes, A. Gupta, M. Rupp and M. B. Ketchen, *Nature (London)* **373**, 225 (1995); D. J. Scalapino, *Phys. Rep.* **250**, 329 (1995); D. Pines, *Phys. C (Amsterdam)* **235-240**, 113 (1994).
- [13] L. C. Rhodes, J. Boker, M. A. Muller, M. Eschrig, and I. M. Ermin, *npj Quantum Mater.* **6**, 45 (2021).
- [14] L. Jiao, S. Howard, S. Ran, Z. Wang, J. O. Rodriguez, M. Sigrist, Z. Wang, N. P. Butch, and V. Madhavan, *Nature (London)* **579**, 523 (2020).
- [15] M. K. Fischer, T. Neupert, C. Platt, A. P. Schnyder, W. Hanke, J. Goryo, R. Thomale, and M. Sigrist, *Phys. Rev. B* **89**, 020509(R) (2014); P. K. Biswas, H. Luetkens, T. Neupert, T. Sturzer, C. Baines, G. Pascua, A. P. Schnyder, M. H. Fischer, J. Goryo, M. R. Lees, H. Maeter, F. Bruckner, H. H. Klauss, M. Nicklas, P. J. Baker, A. D. Hillier, M. Sigrist, A. Amato, D. Johrendt, **87**, 180503 (2013).
- [16] M. Fischer, M. Sigrist, D. F. Agterberg and Y. Yanase, [arXiv:2204.02449](https://arxiv.org/abs/2204.02449); S. Wolf and R. Rachel, *Phys. Rev. B* **102**, 174512 (2020); L. Fu and E. Berg, *Phys. Rev. Lett.* **105**, 097001 (2010); P. A. Frigeri, D. F. Agterberg, A. Koga, and M. Sigrist, **92**, 097001 (2004); V. Kozii and L. Fu, **115**, 207002 (2015).
- [17] C. Kallin and J. Berlinsky, *Rep. Prog. Phys.* **79**, 054502 (2016); A. P. Mackenzie and Y. Maeno, *Rev. Mod. Phys.* **75**, 657 (2003).
- [18] M. S. Foster and A. W. W. Ludwig, *Phys. Rev. B* **77**, 165108 (2008).
- [19] M. Sato, Y. Tanaka, K. Yada, and T. Yokoyama, *Phys. Rev. B* **83**, 224511 (2011).
- [20] Y. Maeno, *Phys. B: Condens. Matter* **280**, 285 (2000); J. Zhang, C. Lorscheer, Q. Gu, and R. A. Klemm, *J. Phys.: Condens. Matter* **26**, 252201 (2014).
- [21] M. Sigrist and K. Ueda, *Rev. Mod. Phys.* **63**, 239 (1991); A. P. Mackenzie and Y. Maeno, *Phys. B (Amsterdam)* **280**, 148 (2000).
- [22] Q. Cheng, B. Jin, and D. Yu, *Phys. Lett. A* **379**, 1172 (2015); T. Yokoyama, Y. Tanaka, and J. Inoue, *Phys. Rev. B* **72**, 220504(R) (2005).
- [23] Q. Cheng, Y. Zhang, K. Zhang, B. Jin, and C. Zhang, *J. Phys.: Condens. Matter* **29**, 085601 (2017).
- [24] Yusuke Nomura, S. Sakai, M. Capone, and R. Arita, *J. Phys.: Condens. Matter* **28**, 153001 (2016).
- [25] Y. Tanaka and S. Kashiwaya, *Phys. Rev. Lett.* **74**, 3451 (1995).
- [26] P. Burset, B. Lu, S. Tamura, and Y. Tanaka, *Phys. Rev. B* **95**, 224502 (2017).
- [27] S. Nakosai, Y. Tanaka, and N. Nagaosa, *Phys. Rev. B* **88**, 180503(R) (2013).
- [28] S. J. Sun, C.-H. Chung, Y.-Y. Chang, W.-F. Tsai, and F.-C. Zhang, *Sci. Rep.* **6**, 24102 (2016); Y. Nishikubo, K. Kudo, and M. Nohara, *J. Phys. Soc. Jpn.* **80**, 055002 (2011).
- [29] N. A. Mortensen, K. Flensberg, and A. P. Jauho, *Phys. Rev. B* **59**, 10176 (1999).
- [30] K. Zhang and Q. Cheng, *Supercond. Sci. Technol.* **31**, 075001 (2018).
- [31] C. Benjamin and J. K. Pachos, *Phys. Rev. B* **78**, 235403 (2008).
- [32] Y. M. Blanter and M. Buttiker, *Phys. Rep.* **336**, 1 (2000).
- [33] M. P. Anantram and S. Datta, *Phys. Rev. B* **53**, 16390 (1996).
- [34] C. Beenakker and C. Schönberger, *Phys. Today* **56(5)**, 37 (2003).
- [35] M. Flöser, D. Feinberg, and R. Melin, *Phys. Rev. B* **88**, 094517 (2013); Martina Flöser, Transport local et non-local: Percolation dans les systemes a effet Hall quantique correlations croisees dans les structures hybrides supraconductrices, Ph.D. thesis, University de Grenoble, 2012.
- [36] G. E. Blonder, M. Tinkham, and T. M. Klapwijk, *Phys. Rev. B* **25**, 4515 (1982).
- [37] L. W. Molenkamp, G. Schmidt, and G. E. W. Bauer, *Phys. Rev. B* **64**, 121202(R) (2001).
- [38] Y. Tanaka, T. Yokoyama, A. V. Balatsky, and N. Nagaosa, *Phys. Rev. B* **79**, 060505(R) (2009); K. Yada, M. Sato, Y. Tanaka, and T. Yokoyama, **83**, 064505 (2011).
- [39] S. Mi, P. Burset, and C. Flindt, *Sci. Rep.* **8**, 16828 (2018).

- [40] We have used *Mathematica* to get the scattering amplitudes after solving the boundary conditions (9) and (12), using which we plot nonlocal conductance, differential shot-noise cross correlations, and HBT correlations. *Mathematica* notebook for the plots for once pairing symmetry ($p_x\hat{z}$) can be found in Github, <https://github.com/TUSARADRI/Shot-noise-in-metal-2D-superconductor-metaljunction.git>.
- [41] S.-B. Zhang and B. Trauzettel, *Phys. Rev. Lett.* **122**, 257701 (2019).
- [42] R. Melin, C. Benjamin, and T. Martin, *Phys. Rev. B* **77**, 094512 (2008).
- [43] M. J. M. de Jong and C. W. J. Beenakker, *Phys. Rev. Lett.* **74**, 1657 (1995); *Phys. Rev. B* **49**, 16070(R) (1994).
- [44] Z. C. Dong, D. Y. Xing, and J. Dong, *J. Phys.: Condens. Matter* **13**, 3839 (2001).
- [45] W. Liming, J.-Y. Luo, X.-X. Cai, K. Sha, C.-P. Yin, and L.-B. Hu, *Front. Phys.* **8**, 50 (2012).
- [46] Y. Liu and Z. Q. Mao, *Phys. C (Amsterdam)* **514**, 339 (2015); A. P. Mackenzie, R. K. W. Haselwimmer, A. W. Tyler, G. G. Lonzarich, Y. Mori, S. Nishizaki and Y. Maeno, *Phys. Rev. Lett.* **80**, 161 (1998).
- [47] R. Melin and D. Feinberg, *Phys. Rev. B* **70**, 174509 (2004).
- [48] G. Bignon, M. Houzet, F. Pistolesi, and F. W. J. Hekking, *Europhys. Lett.* **67**, 110 (2004).
- [49] D. S. Golubev and A. D. Zaikin, *Phys. Rev. B* **99**, 144504 (2019).
- [50] A. O. Denisov, A. V. Bubis, S. U. Piatrusha, N. A. Titova, A. G. Nasibulin, J. Becker, J. Treu, D. Ruhstorfer, G. Koblmüller, E. S. Tikhonov, and V. S. Khrapai, *Semicond. Sci. Technol.* **36**, 09LT04 (2021).
- [51] J. Wei and V. Chandrasekhar, *Nat. Phys.* **6**, 494 (2010).
- [52] A. Das, Y. Ronen, M. Heiblum, D. Mahalu, A. V. Kretinin, and H. Shtrikman, *Nat. Commun.* **3**, 1165 (2012).
- [53] K. M. Bastiaans, D. Cho, T. Benschop, I. Battisti, Y. Huang, M. S. Golden, Q. Dong, Y. Jin, J. Zaanen, and M. P. Allan, *Nat. Phys.* **14**, 1183 (2018).
- [54] Y. C. Liu, F.-C. Zhang, T. M. Rice, and Q.-H. Wang, *npj Quantum Mater.* **2**, 12 (2017).